Chinese Chemical Letters 34 (2023) 107861

Contents lists available at ScienceDirect

Chinese Chemical Letters

journal homepage: www.elsevier.com/locate/cclet

Advanced municipal wastewater treatment and simultaneous energy/resource recovery *via* photo(electro)catalysis

Dengke Wang, Siqi Chen, Shiqin Lai, Weili Dai, Lixia Yang, Lanqing Deng, Mengjuan Suo, Xuyang Wang, Jian-Ping Zou*, Sheng-Lian Luo

Key Laboratory of Jiangxi Province for Persistent Pollutants Control and Resources Recycle, Nanchang Hangkong University, Nanchang 330063, China

ARTICLE INFO

Article history:
Received 30 April 2022
Revised 11 September 2022
Accepted 26 September 2022
Available online 28 September 2022

Keywords:
Wastewater treatment
CO_2 reduction
Hydrogen evolution
Metal recovery
Photo(electro)catalysis

ABSTRACT

Wastewater management and energy/resource recycling have been extensively investigated *via* photo(electro)catalysis. Although both operation processes are driven effectively by the same interfacial charge, each system is practiced separately since they require very different reaction conditions. In this review, we showcase the recent advancements in photo(electro)catalytic process that enables the wastewater treatment and simultaneous energy/resource recovery (WT-ERR). Various literatures based on photo(electro)catalysis for wastewater treatment coupled with CO_2 conversion, H_2 production and heavy metal recovery are summarized. Besides, the fundamentals of photo(electro)catalysis and the influencing factors in such synergistic process are also presented. The essential feature of the catalysis lies in effectively utilizing hole oxidation for pollutant degradation and electron reduction for energy/resource recovery. Although in its infancy, the reviewed technology provides new avenue for developing next-generation wastewater treatment process. Moreover, we expect that this review can stimulate intensive researches to rationally design photo(electro)catalytic systems for environmental remediation accompanied with energy and resource recovery.

1. Introduction

Water pollution has been a common challenge facing people all over the world. Among all the contaminated water, municipal wastewater become one of the toughest stuffs since they have large amount of emissions and contain massive stubborn contaminants [1]. Many technologies have been employed for the municipal wastewater management in recent decades [2,3]. Although some methods take effects toward wastewater remediation, most of them are not considered sustainable because of their long retention time and/or high energy consumption. Besides, the pollutants are simply degraded during the operation processes, and no extra outputs such as energy and resources are recovered from them. Actually, municipal wastewater with typical organic matter concentrations (expressed in chemical oxygen demand, COD) of 400–500 mg COD/L is reported to contain a potential chemical energy of 1.5-1.9 kWh/m^3 of wastewater, which is more than twice the energy demand of a typical activated sludge system [4]. Apart from energy, municipal wastewater also contains tremendous resources like carbon, hydrogen, metal and nutritional ingredients due to the existence of multifarious contaminants. Thus, it was once known as the warehouse of the energy and resources of human. In this scenario, searching and developing a method that can manage wastewater and simultaneously recover energy/resource is highly appealing and become a current hot topic.

According to the final targets, the development course of wastewater-to-energy/resources can be classified into three stages, *i.e.*, water recycling, nitrogen and phosphorus recovery, and carbon, hydrogen and metal recovery. Water recycling is first proposed by researchers since the main component of wastewater is fresh water. Previous studies indicated that almost all the biochemical oxygen demand in municipal water could be removed under the management of activated sludge [5]. Unfortunately, the quality of the recycled water is comparatively low because it contains amounts of inorganic nitrogen and phosphate. Although later use of reverse osmosis membrane technology can improve the quality of reclaimed water, it still consumes a lot of energy [6]. Aiming at eliminating the nitrogen and phosphorus in wastewater, the second evolution stage of wastewater treatment combined with nitrogen/phosphorus recovery is explored. Biological nitrification and denitrification integrated with chemical precipitation are used to realize the recovery of nitrogen and phosphorus [7]. However, large amount of inorganic salts are required during the chemical precip-

* Corresponding author.
E-mail address: zjp_112@126.com (J.-P. Zou).

https://doi.org/10.1016/j.cclet.2022.107861
1001-8417/

itation process, resulting in secondary pollution. Besides, the biological nitrification and denitrification are also energy-intensive processes. Although the first two stages of wastewater treatment can realize the recovery of water, nitrogen and phosphorus, the reclamation of other resources from municipal wastewater is still very limited.

In view of the massive organic pollutants in municipal wastewater, recovering carbon resources from them has gradually been advocated in recent years. In traditional wastewater treatment processes, organic pollutants are finally mineralized into H_2O and CO_2 [8]. However, the evolved CO_2 is one kind of greenhouse gas that causes global warming. Previous studies have shown that CO_2 can be activated and served as an ideal C_1 source for the production of chemical fuels (like CH_4, CH_3OH, C_2H_5OH) [9]. As such, integrating organic pollutant mineralization with CO_2 conversion-to-chemical fuels is of significance. Till now, a few strategies, including anaerobic digestion [10], microbial fuel cells [11], photo(electro)catalysis [12], have been dedicated to realize this target. Among these developed systems, photo(electro)catalysis has been extensively investigated owing to its potential application in environmental remediation and energy/resource conversion [13]. Various redox processes that are thermodynamically either spontaneous or non-spontaneous can be accomplished *via* photo(electro)catalysis under the assistance of extra radiation-induced charges [14]. Taking photocatalysis as an example, photogenerated holes with high oxidation potential in semiconductors can oxidize or even completely mineralize most organic pollutants under illumination [15]. Meanwhile, the photogenerated electrons with sufficiently low potential can fulfill many reduction reactions, *e.g.*, CO_2-to-chemical fuels and H^+-to-renewable energy [16]. To date, a tremendous amount of work has been reported under the implementation of photo(electro)catalysis. And a few reviews focused on energy recovery from wastewater treatment have been reported, providing a detailed perspective of photo/electrocatalysis on the application of such concurrent reactions [17]. In addition to that, metal recovery from wastewater *via* electrocatalysis has also been reviewed, which covers nearly all research articles in this field starting from fundamental and theoretical investigations to applied science [18,19]. However, to the best of our knowledge, there are limited reviews regarding the comprehensive demonstration of wastewater purification and concurrent CO_2-to-chemicals transformations. Additionally, few reviews refer to the effect of compositions and structures of catalysts and pollutants on removal efficiency of organics and recycling efficiency of energy and resources. Therefore, in view of this rapidly advancing field, a critical review summarizing the recent development of wastewater treatment coupled with CO_2-to-chemicals is highly imperative considering the proposal of carbon neutrality that requires the offsetting of CO_2 emission.

Herein, we showcase the recent progress of photo(electro)catalysis in advanced wastewater treatment along with CO_2 conversion. The fundamentals of photo(electro)catalysis on such synergistic reactions are first introduced. Then, the systems focused on organic pollutant degradation coupled with CO_2-to-chemical fuels are discussed. To enrich the theme, the recent progress in photo(electro)catalytic wastewater treatment coupled with H_2 production and heavy metal recovery is also briefly introduced. Moreover, the influence of compositions and structures of photocatalysts and pollutants on such concerted catalytic performance is presented. Finally, a summary and perspective in this hot area of research is cast. Although the application of photo(electro)catalysis in wastewater treatment and simultaneous energy/resource recovery (WT-ERR) is still in its infancy stage, the photo(electro)catalysis have already shown great promise in this field. Therefore, we hope that a review at this time centering on photo(electro)catalytic synchronous reaction can serve as a useful guideline for other researchers to get into this largely unexplored field. Meanwhile, we expect that this review can stimulate intensive researches to rationally design photo(electro)catalytic systems for environmental remediation accompanied with energy and resource recovery.

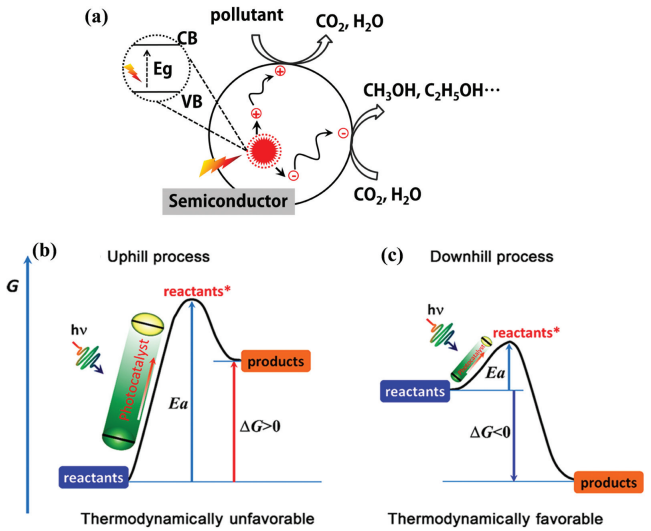

Fig. 1. (a) The energy band and photocatalytic mechanism. Thermodynamics of (b) uphill and (c) downhill photocatalysis. Adapted with permission [24]. Copyright 2017, American Chemical Society.

2. Fundamentals of photo(electro)catalysis on wastewater treatment and simultaneous energy/resource recovery

2.1. Basic principle of photocatalysis on wastewater treatment coupled with energy/resource recovery

Photocatalysis is considered a fascinating approach to alleviate environmental pollution and energy crisis due to its direct utilization of solar energy [20]. Ever since the landmark discovery of a photoelectron-chemical cell using TiO_2-Pt for H_2 evolution by Fujishima and Honda in 1972, chemical reactions initiated by photocatalysis have attracted widespread attention [21]. In general, photocatalytic reactions occur on the surface of semiconductors and are induced by the redox energy bands [22]. To be specific, upon light irradiation, semiconductors will be excited with the transfer of reductive electrons from valence band to conduction band, leaving positive charged holes in the valence band. Driven by internal electric field, the photogenerated electrons and holes afterward are spatially separated and diffuse to the external surface of photocatalyst. Finally, the passionate electrons involve in the reduction reactions while the holes participate in the oxidation reactions (Fig. 1a). Under such established reaction mechanism, most chemical reactions can be realized under the synergy of photogenerated electrons and holes [23].

Given the photocatalytic mechanism, the degradation of organic pollutants and the simultaneous recovery of energy/resources are expected to proceed smoothly over photocatalysts with suitable conduction band and valence band potentials. It is worth mentioning that the efficiency of the whole synergistic reaction still depends on the thermodynamics of different reaction processes since the catalyst cannot change the thermodynamics of the reaction [24]. Photocatalytic degradation of organic pollutants was previously reported as an exothermic reaction, a thermodynamically downhill reaction with negative Gibbs free energy change (Fig. 1b). Oppositely, most reduction reactions, especially water splitting-to-H_2 production and CO_2 reduction, are considered to be uphill reactions, which are thermodynamically unfavorable

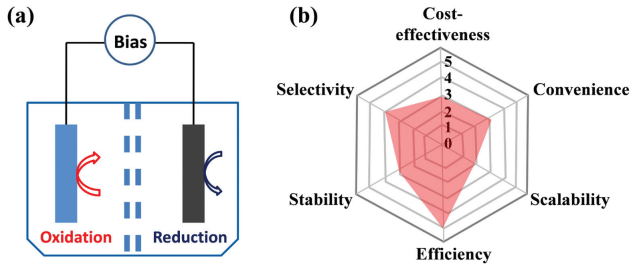

Fig. 2. (a) Electrochemical configurations with proton exchange membrane. (b) Web chart of applicating criteria for particulate electrocatalysis.

(Fig. 1c). In the light of these findings, the recovery process of energy and resources, rather than the degradation process of organic pollutants, is likely the rate-determining step in the synergistic photocatalytic systems. Therefore, much effort has been devoted to accelerating the kinetics of the photo-reduction process.

2.2. Basic principle of electrocatalysis and photoelectrocatalysis on wastewater treatment coupled with energy/resource recovery

Electrocatalysis, a historical technique, plays a central role in environmental remediation [25]. And it becomes one of the most attractive strategies for clean energy conversion thanks to its mild reaction conditions, as well as the eco-friendly driving force by potential synergy with renewable electricity [26]. Usually, the electrocatalytic reactions are carried out in an electrolytic cell, which is mainly composed of anode, cathode, and electrolytes (Fig. 2a). Driven by an applied voltage, the oxidation reaction is performed on the surface of anode while the reduction reaction is involved on the surface of cathode [27]. Due to the *in-situ* oxidation and reduction reactions at anode and cathode respectively, the pollutant oxidation coupled with energy/resources recovery could simultaneously operate in the electrochemical system [12]. In detail, the pollutants are first mineralized into CO_2, H_2O, or free metal ions under anodic oxidation. The as-formed CO_2 or free metal ions afterward diffuse to the cathode and are reduced to chemical fuels and/or metal deposition.

During the redox pair reaction process, the electrocatalyst plays a key role because the rate, efficiency, and selectivity of the reactions cannot keep away from the electrodes [28]. However, the present electrocatalysts are inadequate, and most of them suffer from drawbacks, including low stability, short lifetime, and narrow pH range. Furthermore, the adsorption property of electrodes is often neglected in most cases. An appropriate adsorbing capacity toward substrates will be greatly facilitated their catalytic performance [29]. Accordingly, to design efficient electrocatalysis for wastewater treatment and simultaneous energy/resources recovery, the grand challenge is to develop advanced electrocatalysts.

The efficiency of electrolyzers for wastewater treatment coupled with energy/resource recovery also depends on the electrolyte and bias potential. The bias potential is a sum of standard cell potential ($E^0{}_{cell}$), kinetic overpotentials of cathodic and anodic half-reactions (η_c and η_a), and the ohmic drop (E_Ω) arising from resistance and concentration losses (Eqs. 1–3) [30]. The determination of bias potential should be based on the kinetic overpotentials of the half-reactions. Excessive bias potential will induce serious side reactions at both cathode and anode, reducing current efficiency and increasing energy consumption. The electrolyte in electrolyzers also takes vital role in electrocatalysis [31]. The choice of electrolyte should be carefully considered because the electrolytes probably involve in redox reactions during the catalytic processes. In brief, efficient electrocatalytic systems require the synergy of various factors. A Web diagram summarizing these considerations is shown in Fig. 2b.

$$E(\mathrm{J}) = E^0_{\mathrm{cell}} + E_\Omega(\mathrm{J}) + \eta(\mathrm{J}) \tag{1}$$

$$E^0_{\mathrm{cell}} = E^0_{\mathrm{red}} + E^0_{\mathrm{ox}} = -\frac{\triangle G^0_{\mathrm{reaction}}}{z \times F} \tag{2}$$

$$\triangle G^0_{\mathrm{reaction}} = \sum \upsilon_{\mathrm{p}} \times \triangle G^0_{\mathrm{f.p}} - \sum \upsilon_{\mathrm{r}} \times \triangle G^0_{\mathrm{f.r}} \tag{3}$$

2.3. Evaluation criterion for photo(electro)catalytic wastewater treatment coupled with energy/resource recovery

2.3.1. Degradation rate

Degradation rate of organic pollutant is one of the frequently used indicators to evaluate the efficiency of photo(electro)catalytic wastewater treatment coupled with energy/resource recovery. It is defined as a ratio between degraded amount of pollutants and the total added amount of pollutants (Eq. 4).

$$\text{Degradation rate} = n_{(\text{removed pollutants})}/n_{(\text{the total added pollutants})} \times 100\% \tag{4}$$

However, the degradation rate does not account for the reaction time and catalyst used in the system, making it hard to compare experiments between research labs.

2.3.2. Total organic carbon

The total organic carbon (TOC) is a common indirect measure of organic molecules in wastewater. The decrease of TOC is an important index parameter to evaluate the mineralization degree of organic pollutants in wastewater. And the TOC removal efficiency is defined as the percentage of the removed organic carbon in the total amount of organic carbon found in water, as presented in the following Eq. 5.

$$\text{TOC removal efficiency} = [\text{Removed amount of organic carbon}]/[\text{The total amount of organic carbon}] \times 100\% \tag{5}$$

2.3.3. Faraday efficiency

The Faraday efficiency has become an important criterion to assess the electrocatalytic and photoelectrocatalytic efficiency of energy/resources recovery. According to the electron transfer process of energy and resources production, the Faraday efficiency can be calculated by Eq. 6. In general, the obtained Faraday efficiency is usually referred to the current efficiency (Eq. 7).

$$\text{Faraday efficiency} = [\text{Reacted electrons}]/[\text{The total input electrons}] \times 100\% \tag{6}$$

$$\text{Current efficiency} = zF\xi/It \times 100\% \tag{7}$$

where z represents the stoichiometric coefficient of electron transfer in the reaction. ξ refers to the extent of reaction. I is current intensity. F is Faraday constant and t is the reaction time.

2.3.4. Selectivity

During the half-reaction of energy/resource recovery, the selectivity of the products is another important indicator to measure the catalytic performance (Eq. 8). A highly selective reaction is a long-term goal of the chemical industry, since it can avoid subsequent tedious separation steps.

$$\text{Selectivity} = n_{(\text{target product})}/n_{(\text{the total products})} \times 100\% \tag{8}$$

Table 1
The electrode potential (E^0 *vs.* NHE) of CO_2 reduction with varied products.

Product	Reaction	E^0(V)
$CO_2^{\bullet-}$	$CO_2 + e^- \rightarrow CO_2^{\bullet-}$	−1.85
CO	$CO_2 + 2H^+ + 2e^- \rightarrow CO + H_2O$	−0.51
HCOOH	$CO_2 + 2H^+ + 2e^- \rightarrow HCOOH$	−0.58
CH_2O	$CO_2 + 4H^+ + 4e^- \rightarrow CH_2O + H_2O$	−0.49
CH_3OH	$CO_2 + 6H^+ + 6e^- \rightarrow CH_3OH + H_2O$	−0.39
CH_4	$CO_2 + 8H^+ + 8e^- \rightarrow CH_4 + 2H_2O$	−0.24
C_2H_5OH	$2CO_2 + 12H^+ + 12e^- \rightarrow C_2H_5OH + 3H_2O$	−0.33
C_2H_6	$2CO_2 + 14H^+ + 14e^- \rightarrow C_2H_6 + 4H_2O$	−0.27

Note: E^0 (V *vs.* NHE) are determined under 1 atm gas pressure at room temperature and pH 7 [33,36].

3. Wastewater treatment and simultaneous CO_2 conversion

The complete mineralization of organic pollutants into CO_2 and H_2O is one of the most feasible methods for organic wastewater remediation, because no any other toxic by-products are formed [32]. However, an important but frequently overlooked issue is that CO_2 is one kind of greenhouse gas that, if not handled properly, will cause global warming. Encouragingly, CO_2 is previously regarded as an ideal C_1 source that can be fixed and transferred to organic compounds after activation (Table 1) [33–36]. As such, it is very attractive to mineralize organic pollutants with the combination with CO_2 conversion to value-added chemicals [12,17]. Photo(electro)catalysis has attracted much attention in this field since they are considered promising approach to relieve environmental pollution issues. In this section, organic pollutant degradation coupled with CO_2 conversion through photocatalysis, electrocatalysis, photoelectrocatalysis and their hybrid approaches are summarized to provide a wide survey of the field.

3.1. Photocatalysis

In traditional photocatalytic degradation systems, organic pollutants are mainly decomposed by positive charged holes, while the reductive electrons are often wasted and quenched by O_2 molecules [37]. Instead, it is the reductive electrons, rather than the positively charged holes, take effect on photocatalytic CO_2 conversion [38]. Although both applications are based on the same charge transfer, each system (pollutant degradation or CO_2 reduction) has been practiced separately using different photocatalysts under distinctive conditions. Given that their required potentials are complementary redox pairs, it is highly desirable to combine the photocatalytic organic pollutant degradation and CO_2 reduction, but still challenging. This is because photocatalyst needs to use CO_2 as electron acceptor to oxidize the organic substrates.

Considering that the reactions are predominantly driven by redox energy bands, exploring semiconductors with high valence band and low conduction band are a principal approach to achieve organic pollutant oxidation with concomitant CO_2 reduction [39]. Luo and Suib reported a Vanadium-doped TiO_2 (V-TiO_2) material with high photocatalytic performance of methylene blue (MB) degradation coupled with CO_2 reduction (Fig. 3a) [40]. The partial substitution of Ti^{4+} in TiO_2 with V^{5+} increases the conduction band, and the V^{5+} dopant suppresses the recombination of photogenerated electrons and holes [41]. After 5% V doping, the CO_2 conversion sharply increases with superior CH_3OH and C_2H_5OH production rate of up to about 6.0 and 2.4 μmol g^{-1} h^{-1}, respectively, under solar light irradiation. On behalf of improving the performance, the group further attempted to integrate V-TiO_2 with graphene quantum dots (GQDs) to construct GQDs/V-TiO_2 composite by a hydrothermal method. Due to the unique properties in photosensitization and charge transport, the GQDs are widely reported as cocatalyst for photocatalysis [42,43]. The enhanced visible light absorption, separation efficiency of charge carries and the upconversion properties induced by GQDs make the GQDs/V-TiO_2 system an ideal catalyst for the degradation of organic pollutants and CO_2 reduction. When the loading amount of GQDs is approximately 5%, almost complete MB mineralization is realized and the highest hydrocarbon production for GQDs/V-TiO_2 is obtained with CH_3OH, C_2H_5OH and CH_4 yields measured up to 13.24, 5.65 and 0.445 μmol g^{-1} h^{-1}, respectively (Fig. 3b). More importantly, such reaction can also be performed under visible light irradiation ($\lambda \geq$ 420 nm) (Fig. 3c), thus highlighting the advantages of the hybrid composite.

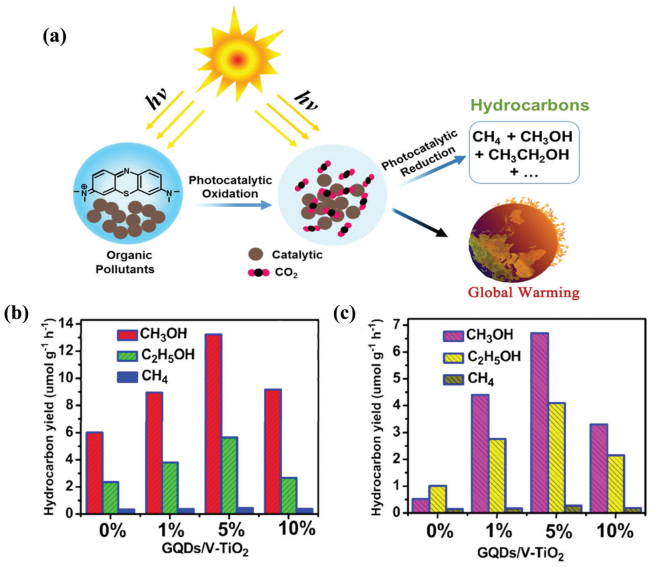

Fig. 3. (a) Schematic illustration of photocatalytic organic pollutant degradation coupled with CO_2 reduction over GQDs/V-TiO_2. The production yields of hydrocarbons over GQDs/V-TiO_2 during the photocatalytic MB degradation and CO_2 reduction under (b) solar light irradiation and (c) visible light irradiation. Reprinted with permission [40]. Copyright 2016, American Chemical Society.

The development of visible-light-responsive photocatalysts to achieve synergistic reactions has attracted the attention of the scientific community [44,45]. Zou and coworkers reported a Fe-doped Ti-based semiconductor ($SrTi_{0.95}Fe_{0.05}O_{3-\delta}$) by a sol-gel method [46]. The prepared $SrTi_{0.95}Fe_{0.05}O_{3-\delta}$ displays strong absorption capacity toward visible light and high charge separation efficiency, showing potential applications in visible-light-induced photocatalysis. Thus, the $SrTi_{0.95}Fe_{0.05}O_{3-\delta}$ composite exhibits higher photocatalytic performance of RhB decomposition and concurrent CO_2-to-hydrocarbons production as compared with bare $SrTiO_3$. Interestingly, the catalytic efficiency is further improved by the modification of $SrTi_{0.95}Fe_{0.05}O_{3-\delta}$ with reduced graphene oxide (RGO). The optimized yields of CH_3OH and C_2H_5OH are up to 10.76 and 6.14 mol g^{-1} h^{-1}, respectively, when 1% RGO is loaded. However, in all cases, the RhB removal rate experienced a maximum value and then decreased. This result stimulates the group to examine the impact of operational variables. They find that the pH value in system manipulates the entire reaction rate. Alkaline environment with high pH value is in favour for CO_2 dissolution and the excessive OH^- ions react with holes to generate $^{\bullet}OH$ radicals [47,48], thereby improving the RhB degradation efficiency as well as reducing the recombination of hole-electron pairs.

In another case, Liu *et al.* reported a bifunctional S-scheme g-C_3N_4/Bi/$BiVO_4$ hybrid photocatalyst by using a substrate-directed liquid phsase deposition combined with $NaBH_4$-induced *in-situ* reduction method, which was used in RhB decomposition and synergistic CO_2 reduction (Fig. 4a) [49]. The feasibility of forming S-scheme heterojunction between g-C_3N_4 and $BiVO_4$ is proofed

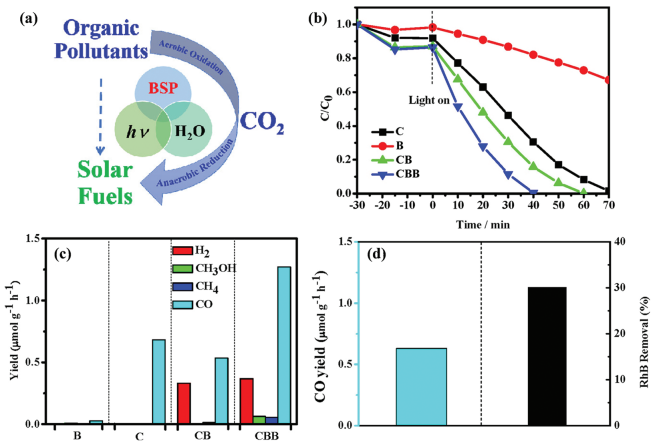

Fig. 4. (a) Schematic illustration of photocatalytic carbon cycling with the combination of aerobic oxidation and anaerobic reduction. (b) Aerobic photocatalytic oxidation of RhB and (c) anaerobic reduction of CO_2 into solar fuels over different catalysts. (d) Photocatalytic performance of RhB oxidation to solar fuels. Reprinted with permission [49]. Copyright 2020, Elsevier.

according to their energy band structures. Density functional theory calculations and scavenger studies verify the electron-bridge function of bismuth nanoparticles at the interface of g-C_3N_4 and $BiVO_4$, leading to greatly enhanced charge transfer and separation efficiency [50,51]. The superiority of g-C_3N_4/Bi/$BiVO_4$ hybrid is first evidenced by the dividual aerobic photocatalytic RhB oxidation and anaerobic photocatalytic CO_2 reduction experiments. High performance with complete RhB degradation is ahieved within 40 min under visible light irradiation (Fig. 4b). Notably, in the CO_2 half-reaction, the g-C_3N_4/Bi/$BiVO_4$ exhibits enhanced performance of CO and H_2 generation rates as compared with g-C_3N_4 and $BiVO_4$ (Fig. 4c). Furthermore, multi-electron reduction products, like CH_4 and CH_3OH, are also generated over C_3N_4/Bi/$BiVO_4$ system, indicating its great potential in CO_2 reduction. Afteward, the catalytic ability of g-C_3N_4/Bi/$BiVO_4$ is further witnessed by the RhB oxidation reaction performed in the anaerobic reaction system with the direct conversion of RhB to solar fuels. Althrough the catalytic efficiency is lower, approximately 30% of RhB degradation and the CO yield of 0.63 μmol g^{-1} h^{-1} are still obtained (Fig. 4d). Since the yields of solar fuels subject to the RhB mineralization rate, the overall photocatalytic RhB-to-solar fuels conversion efficiency can be further improved by promoting the anaerobic RhB oxidation efficiency. This novel bifunctional S-scheme g-C_3N_4/Bi/$BiVO_4$ hybrid photocatalyst system provides new insights for the further development of an integrated aerobic-anaerobic reaction system for photocatalytic carbon cycling from wastewater.

3.2. Electrocatalysis and photoelectrocatalysis

Compared with photocatalysis, electrocatalysis is a more operational method because the redox potential of the electrode can be adjusted by varying the bias potential, electrolytes and different electrode materials [52,53]. In the past decade, great efforts have been devoted to fundamentally investigating design principles [54,55], novel electrodes [56,57] and reactor engineering [58–60] for efficient electrocatalytic reactions. A few works referred to wastewater treatment and simultaneous CO_2 reduction by electrocatalysis have been reported in recent years.

Bharath and coworkers proposed a paired electrolysis strategy that can couple the electrocatalytic CO_2 reduction and MB oxidation [61]. Co_3O_4 nanospheres anchored on nitrogen-doped reduced graphene oxide (Co_3O_4/N-RGO) are prepared *via* a hydrothermal method and employed as electrodes (Fig. 5a). The N-doped RGO in the Co_3O_4/N-RGO hybrid promotes the electrical conductivity and modulates the electron structure of Co atoms in Co_3O_4 to from Co^{2+} [62,63]. The Co^{2+} active species on the surface of the Co_3O_4/N-RGO nanocomposite serves as the catalytic center of CO_2 reduction at cathode, while it also acts as electronic mediator for water oxidation and produces $^{\bullet}OH$ at anode [64]. As such, the Co_3O_4/N-RGO nanocomposite is utilized for bifunctional electrocatalyst and displays great performance in the simultaneous cathodic reduction of CO_2 and anodic oxidation of MB dye in alkaline conditions. An optimal cathodic reduction of CO_2 with 195 μmol L^{-1} cm^{-2} yield of CH_3OH and faradic efficiency of 74.8% is achieved at −0.7 V *vs.* RHE in 1.0 mol/L KOH alkaline solution over 60 min (Figs. 5b-d). Besides, 100% of MB is degraded, highlighting the potential application of reported material as a bifunctional electrocatalyst in pollutant degradation and simultaneous CO_2-to-chemical fuels production (Figs. 5e-g). Since the same reactive sites can induce oxidation and reduction reaction at anode and cathode, this study provides a new insight in preparation bifunctional electrocatalysts for combining cathodic reduction and anodic oxidation.

CO_2 reduction is a thermodynamically unfriendly reaction, and its slow kinetics inhibits the overall efficiency of the synergistic catalysis [65]. To facilitate the whole reaction efficiency, Wang and Wu prepared a series of Sn-based carbon nanotubes doped gas diffusion electrodes (CNT_x/ESGDEs) [66]. Because of the unique layered structure, the employed gas diffusion electrode provides large surface areas for CO_2 adsorption and enhances the mass transfer, clearly benefiting for CO_2 reduction [67,68]. Furthermore, the long-range ordered π-conjugated backbone of the stable carbon nanotubes in the electrode promotes the charge transfer, therefore leading to efficient electrocatalysis [69]. With 40 wt% of carbon nanotube loading, the CNT40/ESGDEs cathode exhibits an optimal conversion rate of CO_2 electroreduction to HCOOH with Faraday efficiency of 69.84%. The maximum organic pollutant removal efficiency (99.34%) was achieved on Ti/SnO_2-Sb anode at a bias potential of −1.8 V *vs.* Ag/AgCl. However, catalytic system shows poor sustainable stability due to the detachment of Sn particles from cathode under high potential, which is a common challenge found in gas diffusion electrode [70,71].

For the purpose of improving the stability of cathode, the same group explored a bismuth-based gas diffusion electrode (EBGDE), which was used for the similar synergistic catalysis (Fig. 6a) [72]. The nanosheet-like morphology of bismuth-based catalysts enables them to be high stable on gas diffusion electrode (Figs. 6b-d). As a consequence, superior performance in terms of both Faraday efficiency (f_{HCOOH}, 91.46%) and COD removal rate (55.25%) over EBGDE-60 is gained in relative to that of Sn-based cathode (69.84% for f_{HCOOH}, 30.12% for COD removal) (Figs. 6e and f) [66]. No obvious decrease in activity after 10 runs highlights the stability of the catalytic system. Noteworthily, the degradation efficacy and COD removal rate of organic pollutant are significantly different when $KHCO_3$ and KCl solutions are used as electrolytes, respectively. The authors explain that only $^{\bullet}OH$ radical mediated oxidation is occurred in the $KHCO_3$ elecctrolyte, whereas extra chlorine species (*e.g.*, Cl_2, HClO, ClO^-) deduced by the reactions between $^{\bullet}OH$ radical and Cl^- in KCl eletrolyte is mutually involved in the pollutant degradation, thus strengthening its catalytic performance [73]. This study give us a better understanding of the electrocatalytic organic pollutant to chemical fuels conversion and also provides some guidance for us in the development of highly efficient electrocatalysis *via* modulating the electrolyte.

Significant advancements of photoelectrocatalysis are also duly reported in the coupling system of CO_2 reduction and organic pollutant degradation [74,75]. Zou *et al.* found that BiOBr film and CuO can be severally used as photoanode and photocathode for TC mineralization and simultaneous CO_2 reduction to chemical fuels under visible light irradiation [76]. The reaction conditions are

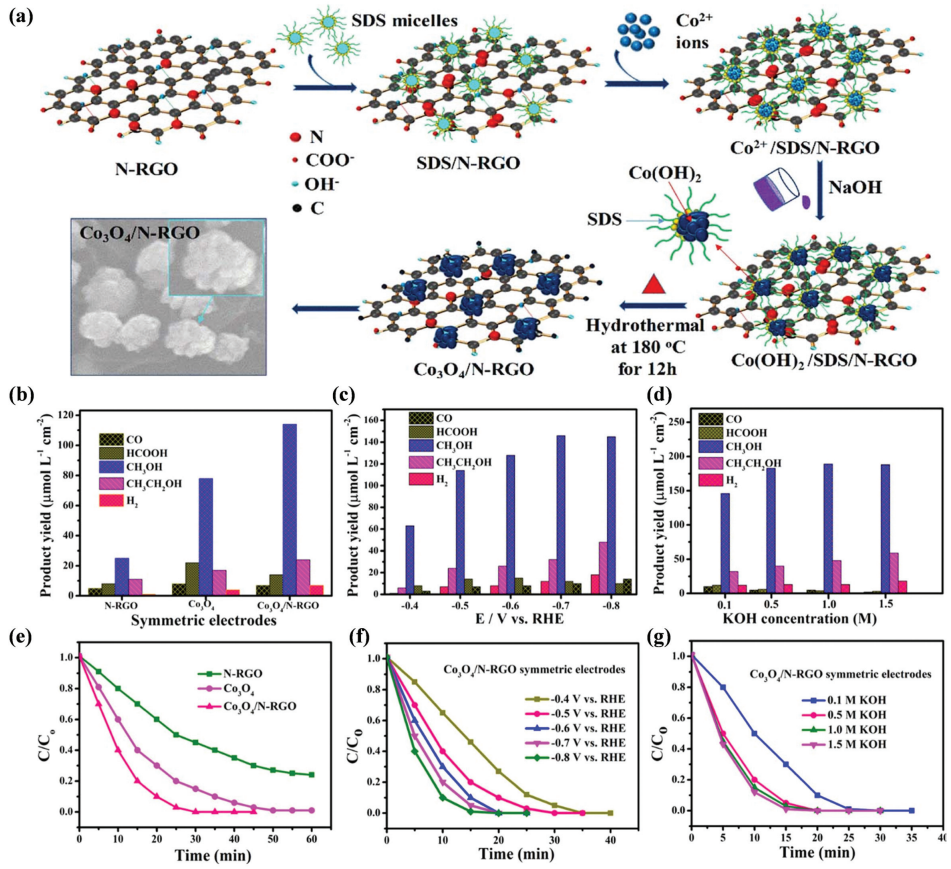

Fig. 5. (a) Schematic illustration for the synthesis of Co_3O_4/N-RGO nanocatalysts. (b-g) The performance of CO_2 reduction and MB dye degradation over different catalysts and reaction conditions. Reprinted with permission [61]. Copyright 2021, American Chemical Society.

Table 2
The degradation efficiency of TC and the yield of liquid fuels over different catalytic systems.

Electrode	Technology	Degradation efficiency of TC (%)	Yield of CH_3OH (μmol/L)	Yield of C_2H_5OH (μmol/L)
BiOBr/Pt	PC	39		
	EC	54		
	PEC	68		
Pt/CuO	PC		9.4	
	EC		70.7	8.3
	PEC		100.3	12.1
BiOBr/CuO	PC	39	9.4	
	EC	63	94.7	11.3
	PEC	80	125.9	26.5

Conditions: For photoelectrocatalysis, anodic chamber containing 0.1 mol/L Na_2SO_4 and 10 ppm TC (80 mL), cathodic chamber containing 0.1 mol/L $KHCO_3$ (80 mL), visible light (>420 nm), applied potential −0.7 V *vs.* AgCl/Ag. For other catalysis, no light was used in electrocatalysis, while no applied potential was added in photocatalysis.

first optimized by individual photoelectrocatalytic TC degradation and CO_2 reduction over BiOBr/Pt and Pt/CuO systems, respectively. Compared with photocatalytic and electrocatalytic systems, the photoelectrocatalytic systems in both TC degradation and CO_2 conversion show superior activities (Table 2). The optimal TC degradation efficiency is up to 68%, while the maximum yields of CH_3OH and C_2H_5OH are 100.3 and 12.1 μmol/L respectively, at the bias potential of −0.7 V *vs.* AgCl/Ag within 2.5 h. Interestingly, the electrocatalytic system composed of BiOBr photoanode and CuO photocathode exhibits higher degradation efficiency of TC and the yield of CO_2 reduction products as compared with BiOBr/Pt system and Pt/CuO system. The TC degradation rate reaches to 80%. And the yields of CH_3OH and C_2H_5OH reach as high as to 125.9 and 26.5 μmol/L, respectively. This work highlights the great potential of photoelectrocatalysis in achieving the one-pot conversion of organic pollutants to liquid fuels by coupling photoelectrocatalytic oxidation and photoelectrocatalytic reduction.

Zheng and Li designed a self-CO_2 recycling photoelectrocatalytic fuel cell system for enhancing the degradation efficiency of pollutants and production yield of carbon-neutral fuel [77]. The system composes of a TiO_2 nanotube photoanode, a cation-exchange membrane and a rotating Ti_3C_2 cathode (Fig. 7a). The anode chamber and the cathode chamber are connected through a switchable gas channel to assist CO_2 transfer. Under the irradiation of 8 W low pressure mercury lamps, 74.8% of methyl orange (MO, 20 mg/L) is degraded on photoanode within 60 min, which shows higher apparent rate constant (0.279 h^{-1}) as compared with that of photocatalytic system (0.156 h^{-1}). Concomitantly, the production of C1 chemical fuel from CO_2 reduction reaction on cathode is achieved, with a total efficiency reaching up to 6.7 μmol g^{-1} h^{-1}. Besides, the organic pollutant reactants in this photoelectrocatalytic system can be extended to MB, Congo red (CR), and tetracycline (TC), highlighting the advantages of this photoelectrocatalytic fuel cell system.

Brito and Zanoni reported a hybrid reactor capable of oxidizing organic pollutant concomitantly with CO_2 reduction to generate chemical fuels using ZrO_2-modified TiO_2 nanotubes (TiO_2Nt-ZrO_2) as photoanode and Cu_2O-doped gas diffusion layer (GDL-Cu_2O) as cathode under UV-vis irradiation (Fig. 7b) [78]. The synthesized TiO_2Nt-ZrO_2 photoanode shows enhanced photocurrent in relative to TiO_2Nt, representing an improvement in the charge separa-

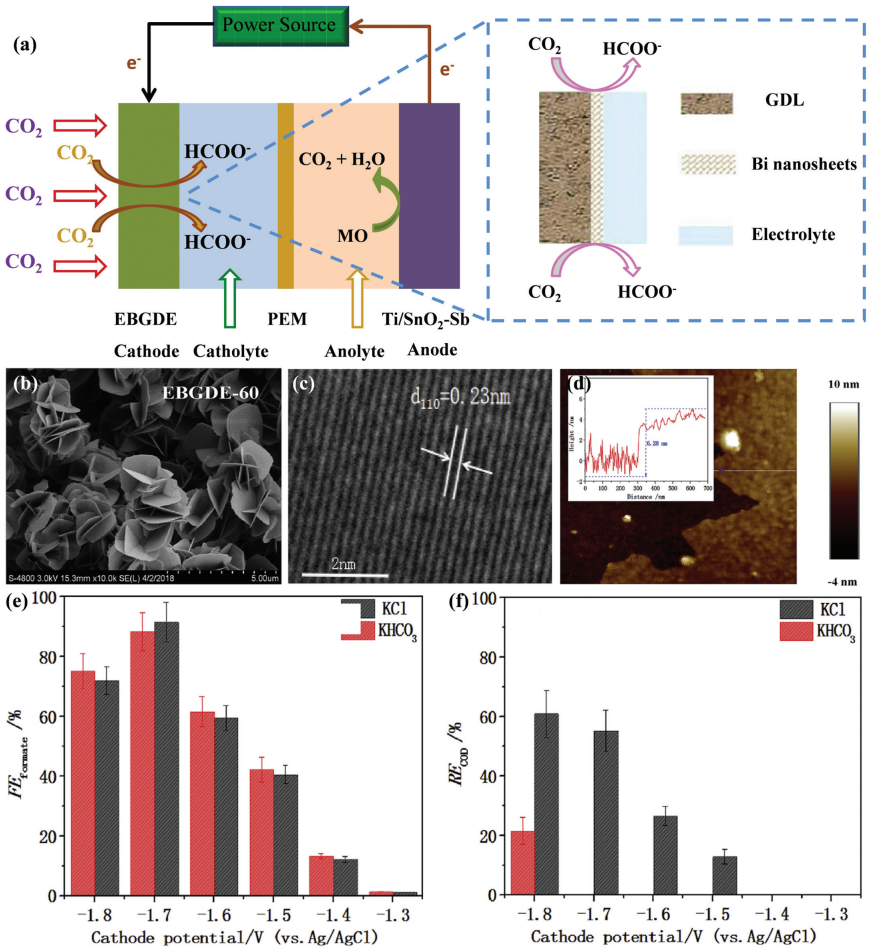

Fig. 6. (a) Scheme of bismuth-based gas diffusion electrode for electrocatalysis. (b) SEM, (c) HRTEM and (d) AFM images of EBGDE-60. (e) Faraday efficiency, (f) COD removal rate and stability of EBGDE-60 for MO degradation to chemical fuels. Reprinted with permission [72]. Copyright 2019, Elsevier.

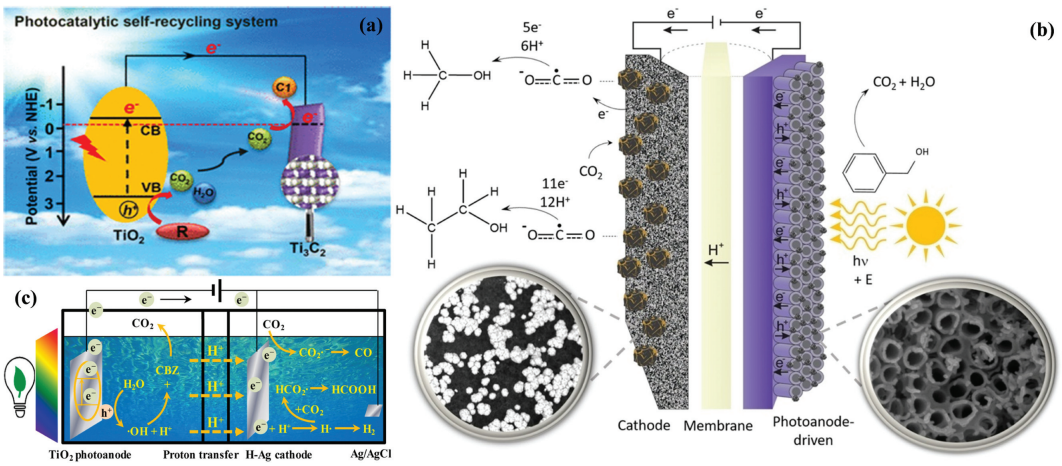

Fig. 7. (a) Schematic diagram of self-CO_2 recycling photoelectrocatalytic fuel cell. Reprinted with permission [77]. Copyright 2020, American Chemical Society. (b) Schematic illustration of photoelectrocatalytic organic pollutant to chemical fuels. Reprinted with permission [78]. Copyright 2019, Elsevier. (c) Schematic diagram of photoelectrocatalytic processes for CBZ degradation, CO_2 reduction and H_2 production using TiO_2 thin film photoanode. Reprinted with permission [79]. Copyright 2021, Elsevier.

tion after light incidence and potential coupling. The optimal benzyl alcohol degradation efficiency reaches 68% over TiO_2Nt-ZrO_2 photoanode with bias potential of 1.5 V *vs.* AgCl/Ag in 0.1 mol/L Na_2SO_7 solution after 180 min, 27% higher than that with TiO_2Nt electrode. Concomitantly, CH_3OH and C_2H_5OH formation at GDL-Cu_2O photocathode attains 3.75 mmol/L and 0.96 mmol/L, respectively. The formation of ethanol increased by 92%, while methanol formation decreased by 24% in TiO_2Nt-ZrO_2/GDL-Cu_2O system after 180 min of electrolysis as compared to that of TiO_2Nt/GDL-Cu_2O system. This study implies that electrode materials take a vital role in photoelectrocatalytic coupling reactions and a proper modification toward electrode will severely facilitate its catalytic performance. In another case, Song and coworkers reported a photoelectrochemical carbamazepine (CBZ) oxidation coupled with si-

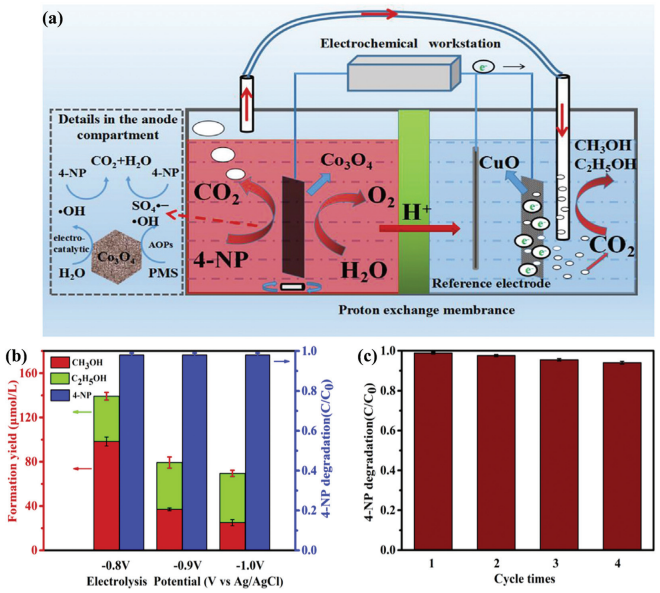

Fig. 8. (a) Schematic illustration of electrocatalysis coupled with AOPs process, (b) catalytic performance and (c) recycling test for synergistic 4-NP degradation to chemicals. Reprinted with permission [83]. Copyright 2019, Elsevier.

multaneous H_2 production and CO_2 conversion to fuels using a TiO_2 thin film as photoanode and Ag plate as cathode (Fig. 7c) [79]. The TiO_2 thin film photoanode is fabricated through a Cl-mediated hydrothermal method combine with calcination processes. The formation of oxygen vacancies and defects on TiO_2 surface after Cl-modification plays significant roles in e^-–h^+ photogeneration and transfer. Thus, the obtained TiO_2 photoanode exhibits superior photoelectrocatalytic capacity. In principle, the Cl-mediated strategy can be used to modify other semiconductors to improve charge transfer, with potential application for photoelectrochemical reactions.

3.3. Electrocatalysis combined with advanced oxidation process

Photo(electro)catalysis combined with other oxidation approaches is proposed as one of the best solutions to tackle the depressed mineralization rate of organics. Previous studies pointed out that advanced oxidation processes (AOPs) was a promising technology for environmental remediation since the generated free radicals from oxidants exhibited high oxidation potential to a broad range of organic pollutants [80,81]. Among various AOPs, persulfate-based AOPs draws extensive attention due to the formation of sulfate radicals ($^{\bullet}SO_4^-$) and hydroxyl radicals ($^{\bullet}OH$) [82].

In one of typical examples, Luo and coworkers recently developed an advanced synergistic catalytic system by coupling electrocatalysis with persulfate-based AOPs for mineralization of 4-NP and CO_2 reduction (Fig. 8a) [83]. Three dimensional-hexagonal Co_3O_4 is employed as anode and flower-like CuO is used as cathode in this system. Since persulfate can be activated by Co species, therefore Co_3O_4 serves not only as an anode material but also as the activator for persulfate [84]. As such, 4-NP in anodic half-cell is mineralized into CO_2 by synergistic effect of electrocatalysis and AOPs. Simultaneously, the CO_2 reduction is occurred on the cathode as the CO_2 gas transferred from anode chamber. After optimizing the reaction conditions, an optimal performance with 4-NP degradation efficiency of 99% is achieved at bias potential of −0.8 V *vs.* AgCl/Ag and pH 6 after 120 min (Figs. 8b and c). While the yields of CH_3OH and C_2H_5OH products are 98.29 and 40.95 mmol/L, respectively, which represents a conversion of 41.8% of 4-NP into liquid fuels and 73.1% electron efficiency. Compared with the pure electrocatalytic system, the system exhibits superior performance, highlighting the great potential of utilization of electrocatalysis coupled with AOPs for wastewater treatment and simultaneous CO_2 conversion.

Remarkably, the entire synergistic catalytic system is influenced by the morphology of electrode materials [85,86]. The authors found that Co_3O_4 with three-dimensional (3D)-hexagonal morphology showed improved removal efficiency of 4-NP as compared to that with a rose-like morphology. Their discussion infers that the superior performance over 3D-hexagonal Co_3O_4 attributes to the larger surface area (127.86 m^2/g) and the unique structure. Except the morphology, the electrode with high stability also affects the overall performance of synergistic catalytic system. In above mentioned system, the CuO cathode undergoes corrosion problem by showing the reduction of CuO to Cu^0, deteriorating the CO_2 reduction performance. Despite the shortcomings, this work provides us a new insight into the electrode designation and the improvement of synergistic catalytic performance.

One year later, the same research group investigated the possibility of using SnO_2 deposited carbon cloth (SnO_2/CC) instead of CuO as cathode for CO_2 reduction coupled with 4-NP degradation, again using Co_3O_4 as anode in the presence of peroxymonosulfate [87]. The lower redox potential of Sn^0/Sn^{2+} (−0.14 V) as compared with that of Cu^0/Cu^+ (0.52 V) enables SnO_2 to show better stability than CuO [88]. Consequently, highly stable catalytic system is obtained and exhibits almost complete 4-NP degradation and considerable Faraday efficiency (24.1%) of CO_2 conversion at bias potential of −1.3 V *vs.* AgCl/Ag.

The above summerized studies highlight great prospect in photo(electro)catalytic organic pollutant degradation and concurrent CO_2 reduction to value-added chemicals. However, in addition to their low efficiency, the CO_2 reduction products (CH_3OH and C_2H_5OH) still leave in solution and are likely to be reversibly oxidized. Moreover, the developed systems cannot be generalized for all organic pollutants since only one or two dyes are investigated as targeted substrates. Therefore, tremendous efforts are still needed to give impetus for photo(electro)catalytically converting organic pollutants to useful chemicals.

4. Wastewater treatment coupled with hydrogen production

H_2 is recognized as renewable energy carrier. Many strategies for H_2 production have been developed, among which water splitting-to-H_2 generation *via* photo(electro)catalysis is the most widely studied [89]. However, most developed photo(electro)catalytic systems rely on excess amounts of sacrificial agents, such as organic acids, alcohols, and amines. The intentional addition of chemicals is not practically acceptable because themselves are another energy/resource and often more expensive than H_2. Since most organic pollutants in wastewater contain abundant electron-rich functional groups that can act as electron donors, these contaminants are expected to act as electron donors during H_2 evolution process [90,91]. In such context, several innovative systems of wastewater decontamination coupled with H_2 production have been constructed in recent years [92–98].

One of the earliest studies in wastewater treatment coupled with H_2 production was conducted using Pt nanoparticles-deposited TiO_2 photocatalyst by Kondarides *et al.* in the early 2000's [99]. The wastewater containing azo-dyes is employed as target object. With 0.5 wt% Pt deposition, the synthesized Pt/TiO_2 realizes an effective H_2 evolution and azo-dyes removal under UV-vis light irradiation (Fig. 9a). Although the activity is greatly affected by the reaction conditions (Figs. 9b-d), this work turns the assumption into reality and provides some guidance for us in the development of efficient TiO_2-based catalytic systems for wastewater treatment and simultaneous energy recovery. Later on, Li *et*

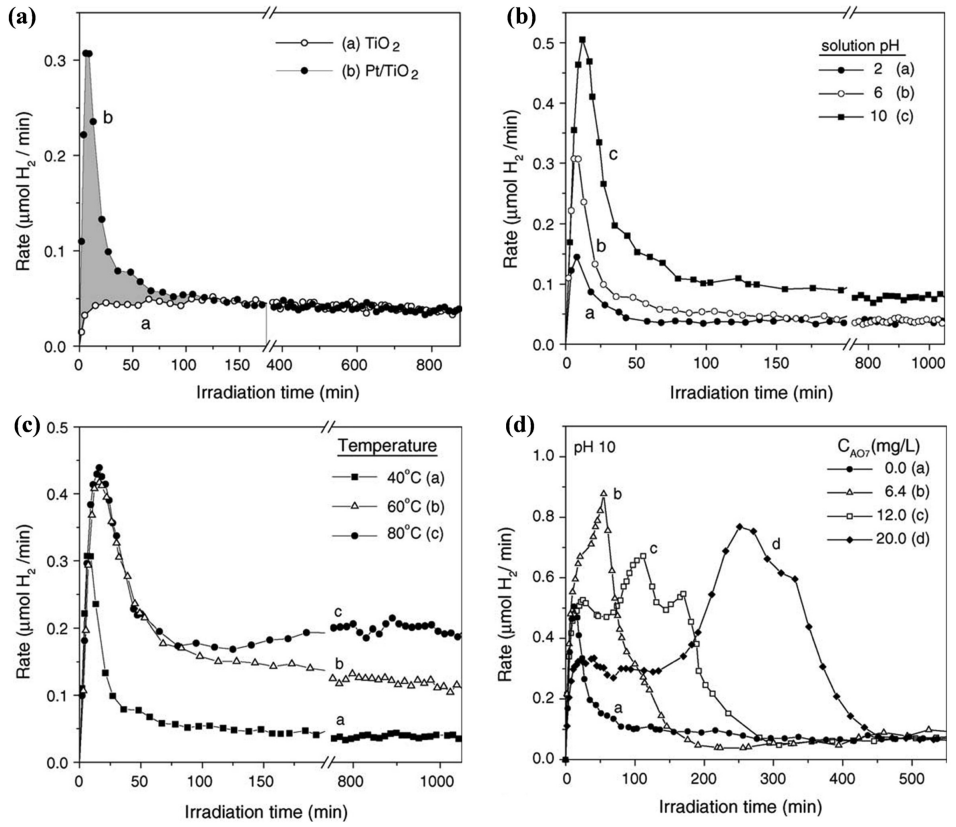

Fig. 9. (a) Organic pollutant degradation integrated with H_2 generation over Pt/TiO_2 and TiO_2. The effect of (b) solution pH, (c) temperature and (d) the concentration of pollutant on performance. Reprinted with permission [99]. Copyright 2005, Elsevier.

al. reported an *in situ* Ti^{3+}-doped TiO_2 nanosheets with dominant (001) facets prepared by supercritical treatment of the precursor obtained from sol-gel hydrolysis of mixed $Ti(n\text{-}OC_4H_9)_4$ and TiF_4 [100]. The doping of Ti^{3+} on the surface of TiO_2 leads to the formation of oxygen vacancies and promotes their light absorption capability, thus conducive to photocatalysis [101–103]. The photocatalytic performance displays that the synthesized Ti^{3+}-doped TiO_2 can cleave water to produce H_2 in the presence of organic pollutants (*i.e.*, *p*-chlorophenol (4-CP), MB, rhodamine B (RhB) and MO), with superior activity over that performed in pure water.

Zou *et al.* designed a ternary composite material composed of graphene quantum dots (GQDs) and g-C_3N_4 co-modified Mn-N-TiO_2 (GQDs/TCN) [104]. In this composite, the surface areas of Mn-N-TiO_2 and the separation efficiency of photogenerated charges are greatly facilitated by the presence of GQDs and g-C_3N_4. The obtained GQDs/TCN photocatalyst exhibits higher photocatalytic organic pollutant degradation and simultaneous H_2 evolution as compared with pristine M-N-TiO_2. In addition, the H_2 evolution rates in the existence of 4-NP, CIP and DEP are all higher than that in pure water over GQDs/TCN system.

Later on, Xing *et al.* synthesized a heterojunction made up of CdS quantum dots (QDs), g-C_3N_4 and carbon dots (CDs) (CDs/CdS/GCN), which was then used for wastewater treatment and simultaneous H_2 production (Fig. 10a) [105]. The as-formed CDs/CdS/GCN composite shows formation of interfaces between CdS QDs and GCN nanosheets leads to an efficient charge separation efficiency. They focus their attention on organic pollutants with different compositions and structures commonly found in printing and dyeing wastewater or pharmaceutical wastewater, such as 4-NP, bisphenol A (BPA) and TC. The photocatalytic system was optimized through variation of the CdS QDs, CDs loading amounts and the initial concentration of pollutants. The optimized

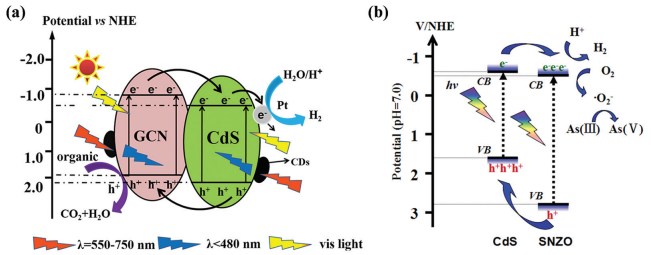

Fig. 10. (a) Schematic illustration of photocatalytic mechanism of CDs/CdS/GCN under light irradiation. Reprinted with permission [105]. Copyright 2018, American Chemical Society. (b) Photocatalytic mechanistic scheme of 30CSNZO under simulated sunlight irradiation. Reprinted with permission [106]. Copyright 2015, American Chemical Society.

3%CDs/10%CdS/GCN composite showed that the H_2 evolution rate in 4-NP solution was lower than that in pure water. However, the H_2 evolution rate in BPA or TC solution was higher than that in pure water.

Apart from H_2 evolution rate, the degradation rates of pollutants also differed between reaction systems. To understand the mechanism of the varied catalytic performance of organic pollutants, the density functional theory (DFT) calculations was investigated. The authors pointed out that the molecular structures and the electron clouds in LUMO (lowest unoccupied molecular orbital) and HOMO (highest occupied molecular orbital) of the organics took significant effect in photocatalytic pollutants degradation along with H_2 evolution. It was noticeable that the system showed relatively high organic pollutant degradation rate and H_2 evolution yield. However, the apparent quantum efficiency of the system was

not reported, which also be a very good indicator of the potential of these photocatalytic systems for large scale application.

Let us move toward a newer type of concerted photocatalysis, which involves the H_2 evolution and simultaneous oxidation of inorganic compounds. Recently, Luo *et al.* reported a coupling reaction system integrating H_2 evolution with As(III) oxidation using heterostructured $CdS/Sr_2(Nb_{17/18}Zn_{1/18})_2O_{7-\delta}$ (CSNZO) composite as photocatalyst (Fig. 10b) [106]. In such heterojunction, CdS has low conduction band for H_2 production [107], while the Zn-doped $Sr_2Nb_2O_7$ possesses high valence band to oxidation As(III). The loading amount of CdS in CSNZO was first optimized by individual photocatalytic H_2 production. The maximum H_2 production rate was observed over 30CSNZO (1.66 mmol h^{-1} g^{-1}), which was higher than those of many semiconductor photocatalysts and even higher than some semiconductor photocatalysts loaded with noble metals. Afterwards, the effect of pH on photocatalytic As(III) oxidation was explored by the optimized 30CSNZO. The result indicated that the photocatalytic oxidation of As(III) over 30CSNZO clearly became more efficient under alkaline conditions (pH 9∼11). Then, the combination of photocatalytic H_2 production and As(III) oxidation was carried out in a solution with varied As(III) concentration (1 mg/L to 10 mg/L) using Na_2S/Na_2SO_3 as sacrificial reagent at pH 9. Unlike the traditional reaction systems that should be conducted under anoxic conditions, in this case the experiments can be performed in the presence of O_2. Interestingly, the H_2 evolution was not inhibited in such aerobic conditions and high evolution rate of 1.24 mmol h^{-1} g^{-1} was still observed. However, the oxidation rate of As(III) was significantly reduced when no O_2 was pumped. This result indicated that O_2 was essential for the oxidation of As(III). In addition, the H_2 evolution rate decreased with the increase of concentration of As(III), suggesting a competition between H_2 evolution and As(III) oxidation. Although the inorganic electron donor (Na_2S/Na_2SO_3) was required, this case was pioneering in this field. Especially, the reaction could be executed under aerobic conditions, indicating its potential practical applications.

5. Wastewater remediation integrated with metal recovery

In addition to organic pollutants, the leakage of heavy metal ions into water circulation system is also an important cause of water pollution [18,108]. Heavy metal ions in wastewater cannot be microbially degraded. It will migrate through water and accumulate in aquatic creature and food, ultimately threatening human health [109]. Therefore, it is urgent to set up a convenient and efficient method for heavy metal ion removal and recovery before its discharge into water environment. As for now, numerous methods have been developed by many reported studies [110,111]. Amongst, photocatalysis, elelectrocatalysis and their comprehensive photoelectrocatalysis are identified as forward-looking technologies for removal and recovery of toxic metal from wastewater since the redox reaction induced by the charge in the interface of catalyst is easily occurred. However, practice shows that the actual process is more complex than a simple metal ion reduction/oxidation [112]. The coexistence of complexing agents (*e.g.*, citrate, nitrilotriacetic acid, cyanide and ethylenediaminetetraacetic acid (EDTA)), makes the management of heavy metal-containing wastewater more complicated. Heavy metal ions can easily complex with those ubiquitous chelating agents to form stable metal complexes with varying structures and toxicity, which are recalcitrant and difficult to remove [113]. Decomplexation of metal complexes *via* photocatalysis, electrocatalysis, and/or photoelectrocatalysis is needed to release heavy metal ions, which require further treatment of removal or recovery [114].

A typical example performed on redox transformation integrated with toxic metal ions' recovery was the simultaneous photoelectrocatalytic oxidation of Cu-EDTA and reductive recovery of Cu^{2+} ions conducted by Liu and colleagues in recent year (Fig. 11a) [115]. TiO_2 film is used as photoanode due to its high decomplexation capability and stability under light irradiation [116]. The catalytic results show that the removal of Cu-EDTA and coinstantaneous Cu recovery on TiO_2 film by photoelectrocatalysis is more efficient than that by individual photocatalysis and electrocatalysis (Fig. 11b). Besides, the Cu^{2+} released by the photoelectrocatalytic degradation of Cu-EDTA do not need to be recovered from the slurry phase through an additional chemical acid extraction process because copper ions are directly deposited on the cathode. Unfortunately, the entire photoelectrocatalytic process is governed by the applied current density as well as the initial pH value as indicated by the controlled experiments (Figs. 11c and d). Although the experimental conditions are optimized, the photoelectrocatalytic oxidation efficiency is still insufficient due to the recalcitrant nature of metal-complexes. Later on, inspired by AOPs, persulfate ($S_2O_8^{2-}$) is added into the photoelectrocatalytic system by Zeng *et al.* to facilitate the oxidation of metal complex [117]. $S_2O_8^{2-}$, a typical peroxide, can be reductively activated into $^{\bullet}SO_4^-$ and $^{\bullet}OH$ when gain an electron from cathode [118]. The *in-situ* formed $^{\bullet}SO_4^-$ and $^{\bullet}OH$ radicals exhibit high oxidation capacity and can decompose a wide range of recalcitrant pollutants [119]. As a result, the constructed photoelectrocatalysis/$S_2O_8^{2-}$ process exhibits improved amount of total organic carbon and oxidation efficiency of Cu-EDTA as compared with single photoelectrocatalytic process (Figs. 11e and f).

Compared to organic matter chelated metal complexes, inorganic ions coordinated metal complexes are more difficult to decompose and recover metals [120]. Taking metallic cyanide as an example, the oxidation of metallic cyanide to release metal ions often accompanies with the generation of highly toxic hydrocyanic acid gas [121,122]. Thus, the oxidation process usually performed under a alkaline condition (pH > 10) to avoid the protonation of cyanide ions. However, the liberated metal ions are easily reductively deposited on cathode, further deteriorating the decomplexation of metal cyanide complexes. To conquer this issue, Zhao and colleagues enquired into the performance of visible light-induced photoelectrocatalytic degradation of copper cyanides with or without EDTA adjuvant under the employment of Bi_2MoO_6 as photoanode [123]. In the absence of adjuvant, cyanide anions are first oxidized into cyanate ions (CNO^-), while synergistic oxidation of Cu^+ to Cu^{2+} is occurred on the photoanode. Because of the basic condition, the oxidized Cu^{2+} and Cu^+ *in situ* hydrolyzed and precipitated on the photoanode, suppressing the further oxidation reaction. Conversely, with the addition of adjuvant ($K_4P_2O_7$), released copper ions are coordinated with EDTA and reductively deposited on the cathode. With this strategy, cyanide could be effectively removed with the simultaneous Cu recovery.

According to above referred studies, the recovery of metallic Cu and removal of the chelators below the legal emission level are hypothesized to be economically and practically feasible. However, despite the low bias potential applied to the photoanode, power consumption is one of the basic parameters that should be critically evaluated for the application of photoelectrocatalytic process to water treatment. Although an outstanding performance for the degradation of pollutants and metal recovery is realized over photoelectrocatalytic process with respect to the electrolytic system, the total energy consumption of photoelectrocatalytic process including the light source should be carefully compared with other photocatalytic and electrolytic systems through technoeconomic analysis.

At present, the treatment of heavy metal-containing wastewater *via* photo(electro)catalysis mostly follows a conventional principle, *i.e.*, the anode chamber oxidizes the organic parts, while the cath-

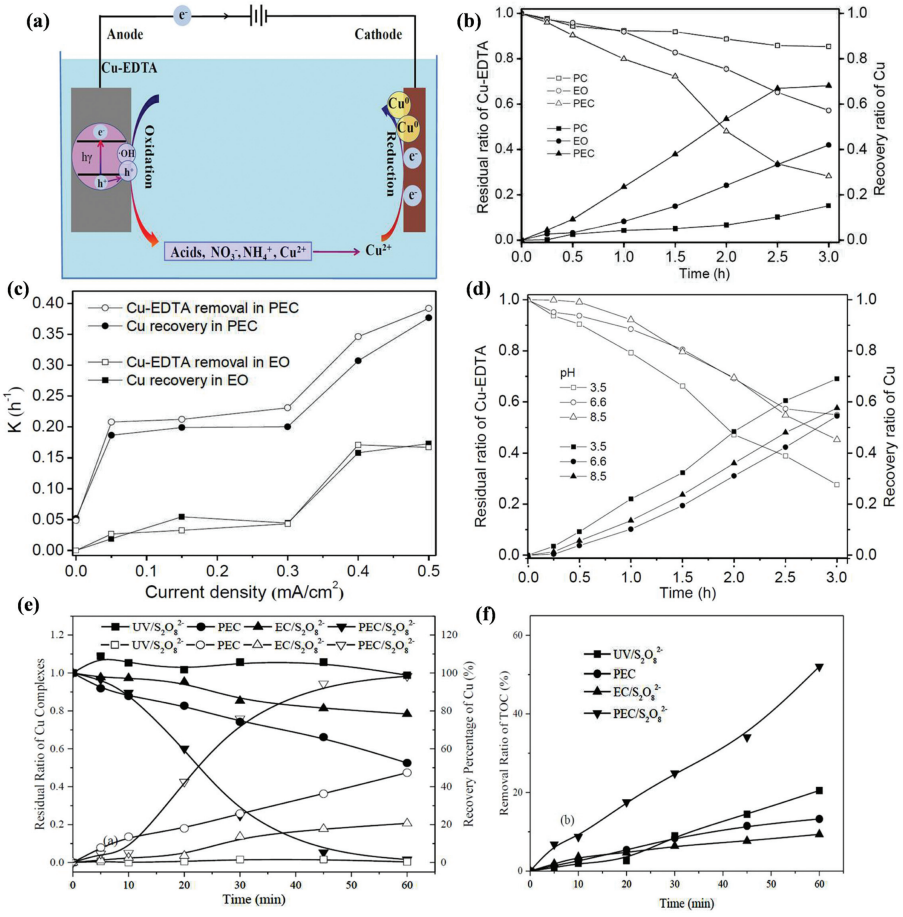

Fig. 11. (a) Schematic illustration of photoelectrocatalytic oxidation of Cu-EDTA and recovery of Cu. (b) Cu-EDTA Removal and Cu recovery over different processes. (c) Kinetic constants of Cu-EDTA and total Cu^{2+} removal. (d) Effect of pH on Cu-EDTA removal and Cu^{2+} recovery over photoelectrocatalysis. Reprinted with permission [115]. Copyright 2013, American Chemical Society. (e) Residual Cu complexes ratio and percentage of Cu recovery and (f) TOC removal ratio in UV/$S_2O_8^{2-}$, photoelectrocatalysis, electrooxidation/$S_2O_8^{2-}$, and photoelectrocatalysis/$S_2O_8^{2-}$ processes. Reprinted with permission [117]. Copyright 2016, American Chemical Society.

ode chamber reduces metal ions. However, several kinds of heavy metal ions show much stronger toxicity in its low valence state as compared to its high valence state like As(III) *vs.* As(V) [124]. As such, a part of heavy metals needs to be oxidized, whereas others require to be reduced.

It is known that Hexavalent U(VI) and trivalent As(III) have radiotoxicity and chemotoxicity, respectively, whereas the As(V) and U(IV) are more environmental-friendly. Therefore, it is necessary to develop methods to efficiently remove the trace amount of U(VI) or As(III) in the water. In this case, photocatalysis combining U(VI) reduction and As(III) oxidation was investigated over an heterostructured g-C_3N_4/TiO_2 (CNT) [125] in recent year. The results show that the concentration of U(VI) and As(III) in the solution rapidly decrease under simulated sunlight irradiation (Fig. 12a). However, the removal rate of U(VI) decrease with the increase of As(III) concentration, whereas the photooxidation rate of As(III) to As(V) increase with the increase of As(III) concentration (Figs. 12b and c). Further mechanism investigation indicates that O_2 is involved in the reaction and play a mediator role in As(III) oxidation coupled with U(VI) reduction (Fig. 12d). The photocatalytic system exhibits good stability and antijamming capability toward co-existing ions (*e.g.*, Na^+, K^+, Mg^{2+}, NO_3^-, Cl^-), highlighting the advantages of the reaction. This study provides us with a new idea of wastewater treatment by coupling metal ion reduction and oxidation process. In the meanwhile, it also prompts us to consider

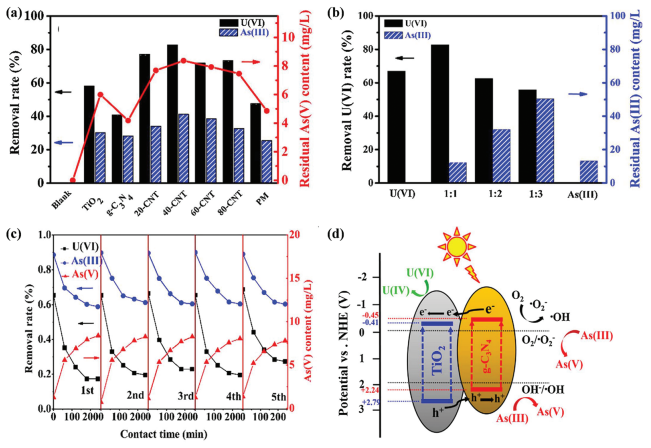

Fig. 12. Removal rate of U(VI) and As(III) over (a) different photocatalysts (b) different U(VI)/As(III) ratio. (c) Cycling test and (d) mechanism of simultaneous removal of U(VI) and As(III) over the 40-CNT under simulated sunlight irradiation. Reprinted with permission [125]. Copyright 2018, Elsevier.

how to design a catalytic system for realizing energy/resources recovery from wastewater treatment in a practical oxygen-containing conditions.

6. Factors affecting photo(electro)catalytic wastewater treatment and concurrent energy/resource recovery

6.1. Effect of general experimental conditions

The performance of WT-ERR is affected by various factors, like the initial concentration of pollutants, pH value, the background constituents in wastewater matrix, the applied potential, the compositions and structures of catalysts/pollutants, and so on [126]. For example, Li *et al.* recently reported that Co_3O_4 modified {001}/{101}-TiO_2 (TC) nanosheets can be used as the efficient dual functional photocatalyst system which can degrade pollutants and simultaneously split water to generate H_2 [127]. Although the unique dual (p-n/surface) heterojunction structure was form between Co_3O_4 and TiO_2 nanosheets that enabled the spatial separation of the charge carriers, both the pollutant degradation and H_2 evolution performance largely depended on the initial concentration of pollutant, pH value, and the background constituents in wastewater matrix. More specifically, with the increase of the initial pollutant (enrofloxacin, ENR) concentrations from 10 mg/L to 50 mg/L, the apparent reaction rate constant decreased from 0.045 min^{-1} to 0.014 min^{-1} due to the limited reactive sites of TC with respect to higher concentrations of ENR. Actually, such a decrease in degradation performance under high pollutant concentration was also evidenced by the Langmuir-Hinshelwood (L-H) model study by showing the linear relationship between ENR degradation efficiency and the L-H kinetic model. Besides, the pH value was also found to be an important parameter on ENR degradation activity since it affected the surface properties of the TC nanosheets and the dissociation of ENR molecules. As mentioned by Li *et al.*, the isoelectric point of TiO_2 is *ca.* 6, while the zwitterion form of ENR set at the pH values between 5.7 and 8.04. In the case of pH values greater than 8.04 or lower than 5.7, the surface of catalysts and ENR molecules carried the same charge, thus the dominant electrostatic repulsion force disfavored the ENR adsorption and degradation process. The author found that the TC nanosheets exhibited the highest photocatalytic activity at a pH of 7.05, which was predominantly controlled by the electrostatic attraction between the surface of catalysts and the ENR molecules.

Furthermore, the background constituents in wastewater matrix play non-negligible role on WT-ERR because they are likely to compete with pollutant molecules to interact with the catalysts. Li *et al.* showed that although NO_3^-, Cl^-, and SO_4^{2-} displayed no apparent influence on ENR degradation, the HCO_3^- exhibited obvious inhibition for the photocatalytic degradation due to its radical quenching effect. Moreover, the divalent cations like Ca^{2+}, Mg^{2+}, and Cu^{2+} ions underwent strong electrostatic interactions with the surface of catalysts, subsequently quenching photogenerated electrons and hampering the photodegradation activity of ENR. Notably, most reported systems are susceptible to the natural organic matter (NOM). However, the current catalytic system was tolerable to the humic acid, indicating its potential application in organic wastewater treatment coupled with energy recovery. Actually, similar influence trend was also observed in the work reported by Fang and Wang [128].

Apart from the abovementioned factors of experimental conditions, a parameter can not be ignored for electrocatalytic and photoelectrocatalytic systems, that is, applied potential. An and Choi disclosed that applied potential played a key role in WO_3 electrode-based *in situ* photoelectrochemical chloride activation for oxidative treatment with simultaneous H_2 evolution under visible light [129]. They found that the higher photocurrent density and higher production of free chlorine species can be obtained as the applied potential bias increased from 0.1 V to 0.9 V (*vs.* Ag/AgCl), thus benefiting for organic pollutant degradation. However, the WO_3 photoanode was less stable at higher bias potential due to the excessive oxidation and reduction. This indicated that a suitable applied potential should be optimized to obtain optimal catalytic performance. In this scenario, it is mandatory to identify the optimum experimental conditions for the WT-ERR applications.

6.2. Effect of surface composition of the catalyst

Compared with the common operating conditions, the physicochemical properties of catalysts and pollutants that are determined by their composition and spatial structure are more complicated [130,131]. They are labeled as the primary factors that are responsible for affecting photo(electro)catalytic WT-ERR. Therefore, a better understanding of the relationship between the composition of catalysts and their activity is important for rational design of synchronous catalytic wastewater treatment and energy/resource recovery. Various organic, inorganic or their combined catalysts with different compositions and structures make them possible to explore their influence on the catalytic activity, yet it is often overlooked by most researchers. The limited results in this field reveal that not only the composition but also the structures of the catalyst affect the performance of water remediation and energy/resource recovery.

For example, Moon and colleagues recently discovered that coupling Co^+-mediated electroreduction and Co^{3+}-mediated electrooxidation processes can be employed for full-electrochemically treating two different volatile organics dichloromethane and phenol [132]. Interestingly, the efficiency in both half-cell is significantly influenced by the electrode materials. Briefly, although Ti, Cu and Ag electrodes show catalytic activity, Ag exhibits the best performance toward $[Co^{II}(CN)_6]^{3-}$ reduction to form reductive Co^+ mediator and disintegration of dichloromethane. The authors ascribed the superiority of Ag to the lower reduction potential as compared to that of Ti and Cu. On the other hand, the efficiency of anode half-cell is also affected by anode materials with Pt electrode by showing the highest yield over the graphite and RuO_2/IrO_2-coated Ti (DSA) anodes. The varied electrocatalytic performance over different electrode materials was understandable since the electroactivity was commonly controlled by specific interaction of reactants with electrode, composition of charged surface sites, and the solution pH. In this case, the distinctive charge transfer kinetics over different electrodes may also be pivotal element corresponding for the divergent electroactivities.

Since most catalysis is a surface chemical process, the reaction performance should be related with the surface properties. To gain insight into how the surface composition and structure influence the catalytic potency, Choi and colleagues developed a photocatalytic system by modifying TiO_2 with F/P and Pt nanoparticles for H_2 production and simultaneously organic pollutants degradation [133,134]. The surface fluorination or phosphation of TiO_2 (F-TiO_2 and P-TiO_2) is taken place by ligand exchange of hydroxyl group on TiO_2 with F^- or phosphates. The zeta potential of TiO_2 after surface modification shifts to more negative values, which is benefit for electrophilic pollutant adsorption [135]. As a result, the surface-modified F-TiO_2/Pt and P-TiO_2/Pt display enhanced activity of simultaneous H_2 evolution and 4-CP and BPA degradations as compared to non-modified TiO_2/Pt (Figs. 13a and b). However, the activity of F-TiO_2/Pt gradually decrease with increasing the pH, ultimately no better than that of Pt/TiO_2 when the pH > 10.5 (Fig. 13c). Conversely, P-TiO_2/Pt generate a significant level of activity over a wide pH range. The author hypothesized that the bidentate complexation of phosphates on the TiO_2 surface was more stable than the monodentate coordinated F^-.

To discover how surface modification influence the activity, the photoinduced charge transfer behavior are investigated by Choi *et al.* The photocurrent onset potential over F-TiO_2 is shifted to more negative values in the presence of urea as compared with that of

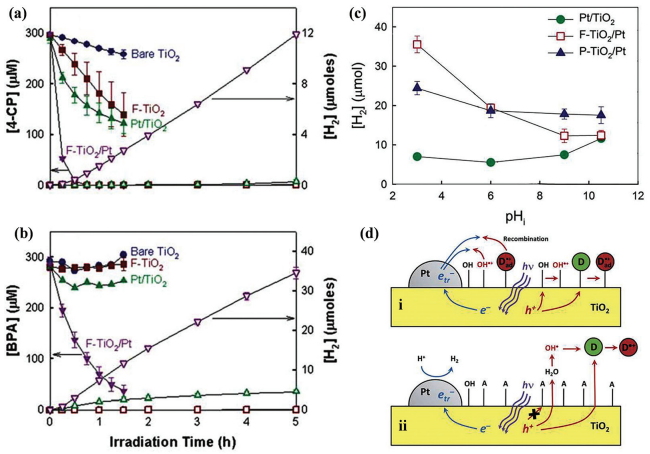

Fig. 13. H_2 production coupled with (a) 4-CP and (b) BPA degradation over different photocatalyst. Reprinted with permission [133]. Copyright 2010, Royal Society of Chemistry. (c) Effect of pH. (d) The interfacial charge transfer mechanism of (i) Pt/TiO_2 and (ii) $F\text{-}TiO_2/Pt$ (or $P\text{-}TiO_2/Pt$). Reprinted with permission [134]. Copyright 2012, Royal Society of Chemistry.

bare TiO_2 and the urea-oxidation photocurrent markedly increase on F–TiO_2 electrode. These observations indicate that the photooxidation of urea was much more efficient on F–TiO_2 than that on bare TiO_2. In addition, F-TiO_2 exhibits a slower open-circuit potential decay in the absence of any electron donor as relative to bare TiO_2, which suggests that the interfacial recombination is retarded by the surface fluorination. This result claims that the surface >Ti–F group acts as an electron-trapping site and reduce interfacial electron transfer rates by tightly holding trapped electrons due to the strong electronegativity of the fluorine [136].

The surface-bounded –OH groups on TiO_2 are reported as chemisorption sites and the hole trapping sites [137]. When the holes are trapped at the –OH sites, they are likely to recombine with electrons trapped nearby. However, as for F-TiO_2 and P-TiO_2, the –OH of TiO_2 is replaced by F or P. The holes can not be able to oxidize F and P. Under this situation, the holes only react with water molecule or organic substrates. Based on these results, a proposed reaction mechanism for synergistic degradation of organic pollutants and production of H_2 is illustrated in Fig. 13d.

From above cases, it can be clearly concluded that the composition of the catalyst indeed take great effect on manipulating the concurrent catalysis. However, the modulating mechanism of the surface in the catalysis is still obscure. The effect of the surface modification reported by Choi *et al.* may not generally fit for all kinds of catalyst and organic substrates since the surface-substrate interaction is very specific to the kind of substrate. Additionally, almost no other influencing factors of catalyst like structure are explored in WT-ERR. To gain more insight into the reaction mechanism between organic substrates and surface of catalyst, great endeavors are still eagerly required.

6.3. Effect of composition and structure of the organic pollutant

For wastewater purification and simultaneous energy/resource recovery, it is not sufficient to only consider the half reaction of proton reduction. It is critical to consider the pollutant destruction reactions since pollutant's composition and spatial structure is another important gist affecting the overall performance. For instance, Hippargi *et al.* discovered that the generation rate of methane and H_2 from carboxylic acid degradation was dramatically varied when different carboxylic acids were used as precursors [138]. As compared with the propionic acid ($pK_a = 4.88$), the acetic acid with $pK_a = 4.78$ was more apt to decompose to generate methane and H_2. Meanwhile, Qu and Jing pointed out that the performance of chlorophenols (CP) degradation and simultaneous H_2 evolution was enslaved to the electronegativity of CP [139]. They found that the rate constant of 2-CP was 2-time higher than that of 3-CP in either H_2 evolution or themselves degradation, and even 4-time than that of 4-CP. Since the physicochemical properties of CP were affected by the substitution position of chlorine functional groups, *ortho*-substituted CP was easier to be activated due to the strong electronegativity of chlorine, thus more convenient for degradation. Actually, such phenomena were also observed in the degradation of phenol, hydroquinone and phloroglucinol as reported by Zhao *et al.* [140]. Excepting for the pK_a and electronegativity of pollutants, the diverse functional groups and spatial orientation in organic pollutants are critical parameters that determine the redox potential and activation energy of bonds. Several research groups once pointed out that apart from physicochemical characters of catalysts, the treatment efficiency of organic pollutants in concerted catalysis could be strongly influenced by the composition and spatial orientation of the organics.

For example, Liu *et al.* recently discovered that the photocatalytic H_2 evolution rates were significantly varied in the presence of RhB, eosin Y, fulvic acid, MB and 4-NP [141]. Moreover, the degradation efficiencies and TOC removal rates of organic pollutants were also different from each other. These indicated that the catalytic performance is also tremendously predetermined by the physicochemical properties of pollutants.

To gain more insight into how organic pollutants influence the performance of concerted catalysis, Zou *et al.* were in recent engaged in the investigation of the effect of composition and spatial orientation of organics on the decomposition and simultaneous H_2 production in a synergistic catalytic system [104]. Graphene quantum dots/Mn-N-TiO_2/g-C_3N_4 (GQDs/TCN) heterostructure was designed and used in photodegradation of organic pollutants (*e.g.*, 4-NP, CIP and DEP) coupled with simultaneous photocatalytic H_2 production. Similar to the observations of Liu *et al.* mentioned above [141], both pollutant degradation efficiency and H_2 evolution rate were varied with different organic pollutants. Specifically, the photocatalytic H_2 evolution rates in the solution of 4-NP, CIP and DEP were all larger than that in pure water system over the 5%GQDs/TCN-0.4 catalyst. And the H_2 evolution rate in the solution of 4-NP was smaller than that in the solutions of CIP and DEP, whereas the photodegradation rate of 4-NP was larger than that of CIP and DEP.

Studies on active species in the catalytic system revealed that different organic pollutants showed different catalytic behaviors toward reactive species. $^{\bullet}OH$ was the main active species for the degradation of 4-NP and CIP, while hole was the main active species for the degradation of DEP. Additionally, the photogenerated electrons also took an effect on the degradation of 4-NP, whereas the degradation of DEP and CIP were hardly affected by electrons. It was believed that the apparent catalytic behaviors of organic pollutants toward different active species were brought by the different constituents and structures of the organics.

To investigate the different photodegradation rates of 4-NP, CIP, and DEP over photocatalyst, the HOMO and LUMO of organic pollutants were calculated by Zou *et al.* (Fig. 14a). According to the calculated results, the highest degradation rate of 4-NP over the GQDs/TCN catalyst could be mainly due to the smaller molecule 4-NP than those of CIP and DEP, leading to more stability of CIP and DEP than 4-NP. The overlapping of electron clouds was identified in the LUMO and HOMO of DEP, which would accelerate the recombination of electrons and holes in these organic molecules. While, the electron clouds in the LUMO and HOMO of CIP were partially separated, leading to better separation of electrons and holes.

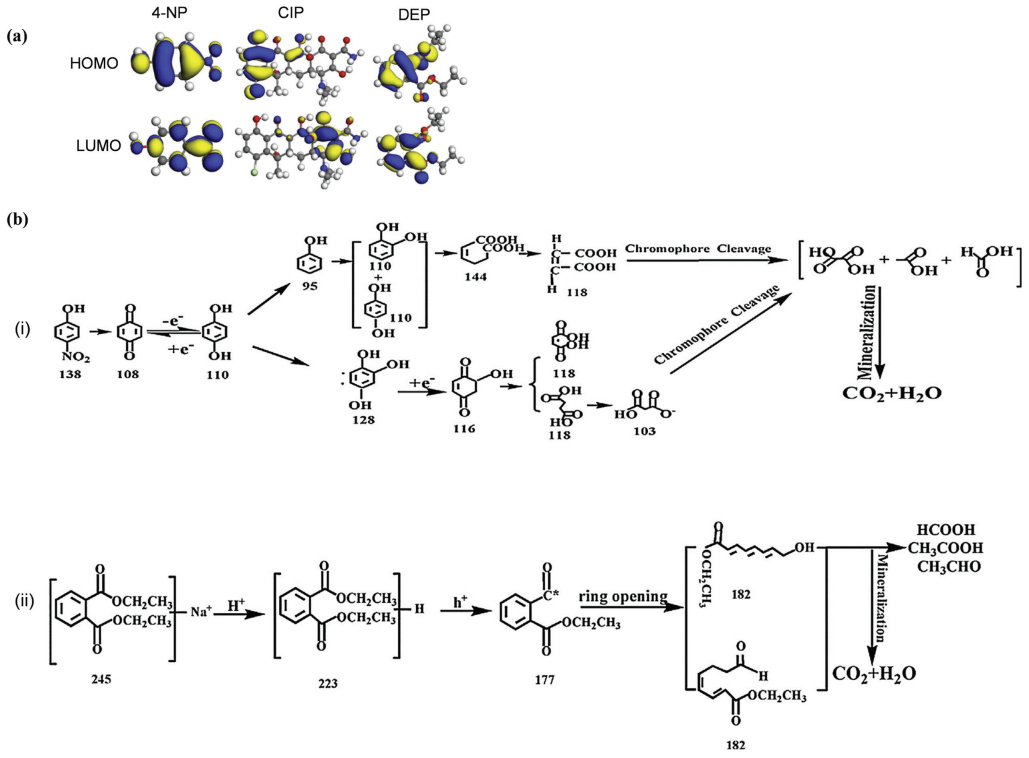

Fig. 14. (a) Frontier electron densities of LUMO and HOMO in different organic pollutants. (b) Degradation pathway of (i) 4-NP and (ii) DEP. Reprinted with permission [104]. Copyright 2018, Elsevier.

To explain why the photocatalytic rate of H_2 production was different in the presence of different organic pollutants, LC-MS tests were further inquired. The results showed that with the extension of photocatalytic time, some hydroxylated and demethylated intermediates would be produced during the degradation of 4-NP. Those intermediates were speculated to further consume electrons according to the authors' discussions. On the contrary, no intermediate products consumed any electrons in the degradation process of DEP. The results well explained that the photocatalytic rate of H_2 evolution in the DEP solution was much higher than that in the 4-NP solution. And the reaction mechanisms of 4-NP and DEP were figured out in Fig. 14b, respectively.

7. Conclusion and perspectives

Wastewater treatment (*e.g.*, pollutant degradation) and energy/resource recovery (*e.g.*, CO_2-to-chemical fuel, H_2 production, and metal recycling) has been extensively investigated by photo(electro)catalysis. Although both processes are relied on the same photo-induced interfacial charge transfers, each reaction system (*e.g.*, pollutant degradation or CO_2-to-chemical fuel) has been practiced separately using different catalytic materials under different experimental conditions. This is because each of them is different in the requirement of charge transfer characteristics. The degradation of organic pollutants is usually initiated by the transfer of VB hole (or $^{\bullet}OH$ radical) under aerobic condition, whereas the CO_2-to-chemical fuel the transfer of CB electrons under the anoxic condition. As thus, it makes the integration of wastewater treatment with energy/resource recovery in an one-pot photo(electro)catalytic system to be a challenge, but it is very promising. By far, under the advocating of carbon neutrality, many studies have tried to design and modify the photoactive materials for this purpose. In this review, we systematically outline the recent innovative advances in WT-ERR *via* photo(electro)catalysis. Three subcatalogs are introduced in this review including wastewater treatment coupled with H_2 evolution, CO_2 conversion, and metal recovery. Furthermore, the fundamental of photo(electro)catalysis and the influence of pollutants and catalysts on the catalytic performance of the CO_2 conversion and/or H_2 evolution is summarized and discussed. Since O_2 is a good electron scavenger, almost every study in the field is carried out under anoxic conditions. In order to bring this field a step closer to real-world applications, it is highly attractive to develop efficient concurrent wastewater treatment and energy/resource recovery system compatible with O_2.

Besides, it is found that the concurrent photo(electro)catalysis of wastewater treatment and energy/resource recovery can be limited by the low efficiency, instability, and high operation cost even at a laboratory scale. Therefore, to substantially facilitate the catalytic performance, the following aspects should be paid more attention.

(a) It is necessary to design and synthesize more efficient and stable catalysts for such a concurrent catalysis. Since the surface chemistry of catalyst governs their redox property, tuning the surface features and increasing the concentration of the active sites are regarded as available strategy for constructing efficient catalyst. At present, the porous materials (*e.g.*, zeolite, metal-organic frameworks, covalent-organic frameworks) are expressed as promising candidates in catalysis due to their inherent large surface areas, uniform but tunable cavities, and tailorable chemistry. In addition, single-atom catalysts with complete exposure of metal atoms have shown great prospects in H_2 evolution and pollutant degradation. Therefore, developing efficient porous materials and single-atom catalysts for photo(electro)catalytic wastewater treatment and simultaneous energy/resource recovery is highly appealing in the future.

(b) The selectivity of reduction products needs to be further modulated. In pollutant degradation coupled with CO_2 conversion system, one can see that CO_2 are commonly reduced to CH_3OH, C_2H_5OH, and CH_4. It is worth noting that gaseous CH_4 can overflow the reaction system, while the liquid CH_3OH and C_2H_5OH remain in the system, which are potentially oxidized back to CO_2. In this context, it is highly expected to be able to selectively regulate the conversion of CO_2 to gaseous CH_4 production.

(c) The catalytic mechanism of wastewater treatment and synergistic energy/resource recovery *via* photo(electro)catalysis is required to be further explored. Despite some active species involved in the concurrent catalysis have been gained, acquiring precise reaction mechanism is still a great challenge due to the migration and transformation mechanism of pollutants remaining unclear. Besides, the surface feature and structure of the catalysts play crucial role in adsorbing and activating pollutants. Therefore, further study should aim at understanding these processes.

(d) To bring it a wider industrial application, more types of pollutants and environmental water matrices are encouraged to be studied. The current researches have been conducted at lab-scale with simulated wastewater containing limited pollutants. Other emerging contaminants (*e.g.*, PPCPs, antibiotics, pesticides, perfluorinated compounds) need to be given more attention in the future. Moreover, due to the influence of external factors (*e.g.*, inorganic ions and natural organic matter), the anti-interference nature of the constructed catalysis needs to explore. And more efforts on anti-interference and high efficiency should be devoted to the environmental water matrices.

Overall, the energy/resource recovery from wastewater *via* photo(electro)catalysis has been demonstrated to be a new opportunities for wastewater re-utilization. Although in its early stage, a bright future for synergetic photo(electro)catalysis in environmental treatment and energy/resource recovery can be envisioned. Considering the diversified categories and structures of catalysts, we believed that efficient semiconductor-based photo(electro)catalytic system for WT-ERR can be realized when all those problems and engineering strategies have been taken into consideration.

Declaration of competing interest

The authors declare that they have no known competing financialinterestsor personal relationships that could have appeared to influence the work reported in this paper.

Acknowledgments

This work was financially supported by the National Natural Science Foundation of China (Nos. 52000097, 51878325, 51868050 and 51938007) and the Natural Science Foundation of Jiangxi Province (Nos. 20192BAB213011 and 20192ACBL21046). Dr. Wang also thanks the Ph.D. research startup foundation of Nanchang Hangkong University (No. EA201802367) and the Open Project Program of the State Key Laboratory of Photocatalysis on Energy and Environment (No. SKLPEE-KF202106), Fuzhou University.

References

[1] N.H. Tran, M. Reinhard, K.Y.H. Gin, Water Res. 133 (2018) 182–207.
[2] P. Chowdhary, A. Raj, R.N. Bharagava, Chemosphere 194 (2018) 229–246.
[3] Z.N. Wang, M.Y. Liu, F. Xiao, et al., Chin. Chem. Lett. 33 (2022) 653–662.
[4] R. Khiewwijit, H. Temmink, H. Rijnaarts, K.J. Keesman, Environ. Model. Softw. 68 (2015) 156–165.
[5] F.Q. Fan, R.H. Xu, D.P. Wang, F.G. Meng, Water Res. 181 (2020) 115915.
[6] Z.W. Zhang, Y.H. Wu, L.W. Luo, et al., Sci. Total Environ. 792 (2021) 148291.
[7] M.N. Hasan, M.M. Altaf, N.A. Khan, et al., Chemosphere 277 (2021) 130328.
[8] J.D. Xiao, Y.B. Xie, J. Rabeah, A. Brückner, H.B. Cao, Acc. Chem. Res. 53 (2020) 1024–1033.
[9] R.C. Ji, J.B. Chen, T.C. Liu, X.F. Zhou, Y.L. Zhang, Chin. Chem. Lett. 33 (2022) 643–652.
[10] Y. Li, Y.G. Chen, J. Wu, Appl. Energy 240 (2019) 120–137.
[11] H.Y. Wang, F. Qian, Y. Li, Nano Energy 8 (2014) 264–273.
[12] T.H. Jeon, M.S. Koo, H. Kim, W. Choi, ACS Catal. 8 (2018) 11542–11563.
[13] J. Highfield, Molecules 20 (2015) 6739–6793.
[14] H.J. Lewerenz, C. Heine, K. Skorupska, et al., Energy Environ. Sci. 3 (2010) 748–760.
[15] Z.D. Wei, J.Y. Liu, W.F. Shangguan, Chin. J. Catal. 41 (2020) 1440–1450.
[16] Q. Wang, K. Domen, Chem. Rev. 120 (2020) 919–985.
[17] S. Kampouri, K.C. Stylianou, ACS Catal. 9 (2019) 4247–4270.
[18] T.O. Ajiboye, O.A. Oyewo, D.C. Onwudiwe, Chemosphere 262 (2021) 128379.
[19] L.M. Yang, W.B. Hu, Z.W. Chang, et al., Environ. Int. 152 (2021) 106512.
[20] L. Candish, K.D. Collins, G.C. Cook, et al., Chem. Rev. 122 (2022) 2907–2980.
[21] A. Fujishima, K. Honda, Nature 238 (1972) 37–38.
[22] Q. Guo, Z.B. Ma, C.Y. Zhou, Z.F. Ren, X.M. Yang, Chem. Rev. 119 (2019) 11020–11041.
[23] T.L. Xia, Y.C. Lin, W.Z. Li, M.T. Ju, Chin. Chem. Lett. 32 (2021) 2975–2984.
[24] F.E. Osterloh, ACS Energy Lett. 2 (2017) 445–453.
[25] C.A. Martínez-Huitle, S. Ferro, Chem. Soc. Rev. 35 (2006) 1324–1340.
[26] G.Q. Zhao, Y.Z. Jiang, S.X. Dou, W.P. Sun, H.G. Pan, Sci. Bull. 66 (2021) 85–96.
[27] H.X. Zhong, M.C. Wang, G.B. Chen, R.H. Dong, X.L. Feng, ACS Nano 16 (2022) 1759–1780.
[28] J. Linnemann, K. Kanokkanchana, K. Tschulik, ACS Catal. 11 (2021) 5318–5346.
[29] L. Rebollar, S. Intikhab, N.J. Oliveira, et al., ACS Catal. 10 (2020) 14747–14762.
[30] X.V. Medvedeva, J.J. Medvedev, S.W. Tatarchuk, R.M. Choueiri, A. Klinkova, Green Chem. 22 (2020) 4456–4462.
[31] Y.L. Quan, J.X. Zhu, G.F. Zheng, Small 1 (2021) 2100043.
[32] D. Shahidi, R. Roy, A. Azzouz, Appl. Catal. B: Environ. 174 (2015) 277–292.
[33] S.Z. Xu, E.A. Carter, Chem. Rev. 119 (2019) 6631–6669.
[34] B.M. Tackett, E. Gomez, J.G. Chen, Nat. Catal. 2 (2019) 381–386.
[35] P. Prabhu, V. Jose, J.M. Lee, Adv. Funct. Mater. 30 (2020) 1910768.
[36] X.X. Chang, T. Wang, J.L. Gong, Energy Environ. Sci. 9 (2016) 2177–2196.
[37] D.N. Jiang, P. Xu, H. Wang, et al., Coordin. Chem. Rev. 376 (2018) 449–466.
[38] Z.J. Wang, H. Song, H.M. Liu, J.H. Ye, Angew. Chem. Int. Ed. 59 (2020) 8016–8035.
[39] M. Melchionna, P. Fornasiero, ACS Catal. 10 (2020) 5493–5501.
[40] J.P. Zou, D.D. Wu, J.M. Luo, et al., ACS Catal. 6 (2016) 6861–6867.
[41] G. Rossi, L. Pasquini, D. Catone, et al., Appl. Catal. B: Environ. 237 (2018) 603–612.
[42] Y.B. Yan, J. Gong, J. Chen, et al., Adv. Mater. 31 (2019) 1808283.
[43] V.C. Hoang, K. Dave, V.G. Gomes, Nano Energy 66 (2019) 104093.
[44] Y. Yamaguchi, A. Kudo, Front. Energy 15 (2021) 568–576.
[45] R. Acharya, K. Parida, J. Environ. Chem. Eng. 8 (2020) 103896.
[46] W.H. Dong, D.D. Wu, J.M. Luo, et al., J. Catal. 349 (2017) 218–225.
[47] X. Lu, C.Q. Zhu, Z.S. Wu, et al., J. Am. Chem. Soc. 142 (2020) 15438–15444.
[48] D.A. Henckel, M.J. Counihan, H.E. Holmes, et al., ACS Catal. 11 (2021) 255–263.
[49] Q. Xie, W.M. He, S.W. Liu, Chin. J. Catal. 41 (2020) 140–153.
[50] M.F.R. Samsudin, H. Ullah, R. Bashiri, et al., ACS Sustain. Chem. Eng. 8 (2020) 9393–9403.
[51] Y. Wang, G.Q. Tan, T. Liu, et al., Appl. Catal. B: Environ. 234 (2018) 37–49.
[52] R.Z. Zhang, B.Y. Wu, Q. Li, et al., Coordin. Chem. Rev. 422 (2020) 213436.
[53] L. Zhang, Z.J. Zhao, T. Wang, J.L. Gong, Chem. Soc. Rev. 47 (2018) 5423–5443.
[54] Z.W. Seh, J. Kibsgaard, C.F. Dickens, et al., Science 355 (2017) eaad4998.
[55] F. Franco, C. Rettenmaier, H.S. Jeon, B.R. Cuenya, Chem. Soc. Rev. 49 (2020) 6884–6946.
[56] Q. Lu, J. Rosen, Y. Zhou, et al., Nat. Commun. 5 (2014) 3242.
[57] J. Rosen, G.S. Hutchings, Q. Lu, et al., ACS Catal. 5 (2015) 4586–4591.
[58] D.S. Ripatti, T.R. Veltman, M.W. Kanan, Joule 3 (2019) 240–256.
[59] S. Verma, X. Lu, S.C. Ma, R.I. Masel, P.J. Kenis, Phys. Chem. Chem. Phys. 18 (2016) 7075–7084.
[60] D.M. Weekes, D.A. Salvatore, A. Reyes, A. Huang, C. Berlinguette, Acc. Chem. Res. 51 (2018) 910–918.
[61] G. Bharath, K. Rambabu, C. Aubry, et al., ACS Appl. Energy Mater. 4 (2021) 11408–11418.
[62] Y.K. Long, J. Dai, S.Y. Zhao, et al., Environ. Sci. Technol. 55 (2021) 5357–5370.
[63] Y.L. Chen, X. Bai, Y.T. Ji, T. Shen, Chem. Eng. J. 430 (2022) 132951.
[64] L. Wang, J.W. Wan, Y.S. Zhao, N.L. Yang, D. Wang, J. Am. Chem. Soc. 141 (2019) 2238–2241.
[65] W.C. Lai, Z.S. Ma, J.W. Zhang, et al., Adv. Func. Mater. 32 (2022) 2111193.
[66] Q.N. Wang, X.Q. Wang, C. Wu, Y.Y. Cheng, Q.Y. Sun, H.B. Yu, J. CO_2 Util. 26 (2018) 425–433.
[67] T.N. Nguyen, C.T. Dinh, Chem. Soc. Rev. 49 (2020) 7488–7504.
[68] H. Rabiee, L. Ge, X.Q. Zhang, et al., Energy Environ. Sci. 14 (2021) 1959–2008.
[69] H. Dong, M. Lu, Y. Wang, et al., Appl. Catal. B: Environ. 303 (2022) 120897.
[70] M.L. Zhang, Z.D. Zhang, Z.H. Zhao, et al., ACS Catal. 11 (2021) 11103–11108.
[71] W.F. Xie, H. Li, G.Q. Cui, et al., Angew. Chem. Int. Ed. 60 (2021) 7382–7388.
[72] Q.N. Wang, C.Q. Zhu, C. Wu, H.B. Yu, Electrochim. Acta 319 (2019) 138–147.
[73] J. Wu, K. Zhu, H. Xu, W. Yan, Chin. J. Catal. 40 (2019) 917–927.
[74] N. Nandal, S.L. Jain, Coordin. Chem. Rev. 451 (2022) 214271.
[75] E. Kusmierek, Catalysts 10 (2020) 439.
[76] S.S. Liu, Q.J. Xing, Y. Chen, et al., ACS Sustain. Chem. Eng. 7 (2019) 1250–1259.

[77] J. Zhang, S. Lv, J.L. Zheng, et al., ACS Sustain. Chem. Eng. 8 (2020) 11133–11140.
[78] J.F. de Brito, J.A.L. Perini, S. Perathoner, M.V.B. Zanoni, Electrochim. Acta 306 (2019) 277–284.
[79] D. Wang, Y.N. He, N. Zhong, et al., J. Hazard. Mater. 410 (2021) 124563.
[80] D.B. Miklos, C. Remy, M. Jekel, et al., Water Res. 139 (2018) 118–131.
[81] X.G. Duan, H.Q. Sun, S.B. Wang, Acc. Chem. Res. 51 (2018) 678–687.
[82] J. Lee, U. von Gunten, J.H. Kim, Environ. Sci. Technol. 54 (2020) 3064–3081.
[83] J.P. Zou, Y. Chen, S.S. Liu, et al., Water Res. 150 (2019) 330–339.
[84] W.D. Oh, Z.L. Dong, T.T. Lim, Appl. Catal. B: Environ. 194 (2016) 169–201.
[85] R. Cheula, M. Maestri, G. Mpourmpakis, ACS Catal. 10 (2020) 6149–6158.
[86] H.Y. Tan, J. Wang, S.Z. Yu, K.B. Zhou, Environ. Sci. Technol. 49 (2015) 8675–8682.
[87] M. Zhu, L.S. Zhang, S.S. Liu, et al., Chin. Chem. Lett. 31 (2020) 1961–1965.
[88] J. Wang, W. Liu, D.M. Li, Y.P. Wang, J. Alloy. Compd. 588 (2014) 378–383.
[89] Z. Wang, C. Li, K. Domen, Chem. Soc. Rev. 48 (2019) 2109–2125.
[90] L. Wang, X.L. Geng, L. Zhang, et al., Chemosphere 286 (2022) 131558.
[91] C.G. Liu, Z.F. Lei, Y.N. Yang, Z.Y. Zhang, Water Res. 47 (2013) 49586–49592.
[92] X.J. Zheng, C.L. Li, M. Zhao, et al., Int. J. Hydrog. Energy 42 (2017) 7917–7929.
[93] Y. Rong, L. Tang, Y.H. Song, et al., RSC Adv. 6 (2016) 80595–80603.
[94] K.H. Chu, L.Q. Ye, W. Wang, et al., Chemosphere 183 (2016) 219–228.
[95] L. He, L. Li, T.T. Wang, et al., Dalton Trans. 43 (2014) 16981–16985.
[96] R. Shwetharani, M. Sakar, H.R. Chandan, R.G. Balakrishna, Mater. Lett. 218 (2018) 262–265.
[97] Y.P. Peng, H.L. Chen, C.P. Huang, Appl. Catal. B: Environ. 209 (2017) 437–446.
[98] J. Han, Y.R. Bian, X.Z. Zheng, X.M. Sun, L.W. Zhang, Chin. Chem. Lett. 28 (2017) 2239–2243.
[99] A. Patsoura, D.I. Kondarides, X.E. Verykios, Appl. Catal. B: Environ. 64 (2006) 171–179.
[100] J.G. Wang, P. Zhang, X. Li, J. Zhu, H.X. Li, Appl. Catal. B: Environ. 134-135 (2013) 198–204.
[101] M.Q. Hu, Z.P. Xing, Y. Cao, et al., Appl. Catal. B: Environ. 226 (2018) 499–508.
[102] K.X. Li, Z.X. Zeng, L.S. Yan, et al., Appl. Catal. B: Environ. 187 (2016) 269–280.
[103] H. Park, A. Bak, Y.Y. Ahn, J. Choi, M.R. Hoffmannn, J. Hazard. Mater. 211-212 (2012) 47–54.
[104] Y.C. Nie, F. Yu, L.C. Wang, et al., Appl. Catal. B: Environ. 227 (2018) 312–321.
[105] X.H. Jiang, L.C. Wang, F. Yu, et al., ACS Sustain. Chem. Eng. 6 (2018) 12695–12705.
[106] J.P. Zou, D.D. Wu, S.K. Bao, et al., ACS Appl. Mater. Interfaces 7 (2015) 28429–28437.
[107] D.K. Wang, H. Zeng, X. Xiong, et al., Sci. Bull. 65 (2020) 113–122.
[108] F. Lu, D. Astruc, Coordin. Chem. Rev. 356 (2018) 147–164.
[109] K. Vikrant, K.H. Kim, Chem. Eng. J. 358 (2019) 264–282.
[110] J.J. Rueda-Marquez, I. Levchuk, P.F. Ibanez, M. Sillanpaa, J. Clean. Prod. 258 (2020) 120694.
[111] S. Al-Amshawee, M.Y.B.M. Yunus, A.A.M. Azoddein, et al., Chem. Eng. J. 380 (2020) 122231.
[112] G.R. Xu, Z.H. An, K. Xu, et al., Coordin. Chem. Rev. 427 (2021) 213554.
[113] Y. Zhu, W.H. Fan, T.T. Zhou, X.M. Li, Sci. Total Environ. 678 (2019) 253–266.
[114] Z. Xu, Q.R. Zhang, X.C. Li, X.F. Huang, Chem. Eng. J. 429 (2022) 131688.
[115] X. Zhao, L.B. Guo, B.F. Zhang, H.J. Liu, J.H. Qu, Environ. Sci. Technol. 47 (2013) 4480–4488.
[116] F. Zhang, W.L. Wang, C.Z. Zhou, Y.L. Sun, J.F. Niu, Chemosphere 278 (2021) 130465.
[117] H.B. Zeng, S.S. Liu, B.Y. Chai, et al., Environ. Sci. Technol. 50 (2016) 6459–6466.
[118] Z H, W.Q.Guo Wang, B.H. Liu, et al., Water Res. 160 (2019) 405–414.
[119] D.K. Wang, H. Zeng, S.Q. Chen, J. Catal. 406 (2022) 1–8.
[120] L. Tian, P. Chen, X.H. Jiang, et al., Water Res. 209 (2022) 117890.
[121] S.C. Tian, C.Z. Dang, R. Mao, X. Zhao, ACS Sustain. Chem. Eng. 6 (2018) 10273–10281.
[122] K. Xiao, B. Zhou, S.Y. Chen, et al., Electrochem. Commun. 100 (2019) 34–38.
[123] X. Zhao, J.J. Zhang, M. Qiao, H.J. Liu, J.H. Qu, Environ. Sci. Technol. 49 (2015) 4567–4574.
[124] K.H. Xue, J. Wang, R. He, et al., Sci. Total Environ. 732 (2020) 138963.
[125] X.H. Jiang, Q.J. Xing, X.B. Luo, et al., Appl. Catal. B: Environ. 228 (2018) 29–38.
[126] J.M. Luo, S.Q. Zhang, M. Sun, et al., ACS Nano 13 (2019) 9811–9840.
[127] Y.Y. Wu, Y.Q. Li, H.J. Hu, G.S. Zeng, C.H. Li, ACS ES&T Eng. 1 (2021) 603–611.
[128] X.X. Ma, X.K. Liu, J.H. Tang, et al., Appl. Surf. Sci. 602 (2022) 154276.
[129] M.S. Koo, X.F. Chen, K. Cho, T.C. An, W. Choi, Environ. Sci. Technol. 53 (2019) 9926–9936.
[130] X.H. Jiang, L.S. Zhang, H.Y. Liu, et al., Angew. Chem. Int. Ed. 59 (2020) 23112–23116.
[131] L.S. Zhang, X.H. Jiang, Z.A. Zhong, et al., Angew. Chem. Int. Ed. 60 (2021) 21751–21755.
[132] M. Govindan, K.C. Pillai, B. Subramanian, I.S. Moon, ACS Omega 2 (2017) 3562–3571.
[133] J. Kim, W. Choi, Energy Environ. Sci. 6 (2010) 1042–1045.
[134] J. Kim, D. Monllor-Satoca, W. Choi, Energy Environ. Sci. 5 (2012) 7647–7656.
[135] G. Iervolino, V. Vaiano, J.J. Murcia, et al., J. Catal. 339 (2016) 47–56.
[136] D. Monllor-Satoca, R. Gómez, J. Phys. Chem. C 112 (2008) 139–147.
[137] A. Heuer-Jungemann, N. Feliu, I. Bakaimi, et al., Chem. Rev. 119 (2019) 4819–4880.
[138] G. Hippargi, S. Anjankar, R.J. Krupadam, S.S. Rayalu, Fuel 291 (2021) 120113.
[139] N. Sun, Y. Qu, C.H. Yang, et al., Appl. Catal. B: Environ. 263 (2020) 118313.
[140] Z.Y. Wu, Z.Y. Zhou, Y.J. Zhang, et al., Electrochim. Acta 254 (2017) 140–147.
[141] S.Q. Zhang, L.L. Wang, C.B. Liu, et al., Water Res. 121 (2017) 11–19.